

Association Euratom - Risø National Laboratory Annual Progress Report 1994

**Edited by J. P. Lynov, P. Michelsen
and B. N. Singh**

Risø National Laboratory, Roskilde, Denmark
June 1995
VOL 25 No 24

Risø-R-830(EN)

Association Euratom - Risø National Laboratory Annual Progress Report 1994

**Edited by J. P. Lynov, P. Michelsen
and B. N. Singh**

**Risø National Laboratory, Roskilde, Denmark
June 1995**

Abstract The program of the Research Unit of the Fusion Association Euratom - Risø National Laboratory covers work in fusion plasma physics and in fusion technology. The fusion plasma physics group has activities within (a) studies of nonlinear dynamical processes in magnetized plasmas, (b) development of laser diagnostics for fusion plasmas, and (c) development of pellet injectors for fusion experiments. The activities in technology cover (a) radiation damage of fusion reactor materials and (b) water radiolysis under ITER conditions. A summary of the activities in 1994 is presented.

ISBN 87-550-2084-4
ISSN 0106-2840

Grafisk Service · Risø · 1995

Contents

1	Preface	5
2	Work in Fusion Plasma Physics	6
2.1	Nonlinear Dynamics of Fusion Plasmas	6
2.1.1	Introduction	6
2.1.2	Coherent Structures and Transport in Drift-wave Turbulence	7
2.1.3	Investigations of η_i -vortices and Turbulence	7
2.1.4	Self-organization in Two-dimensional Circular Shear Layers	8
2.1.5	The Temporal Evolution of the Lamb Dipole	8
2.1.6	Formation of Dipolar Vortices by Self-organization in Two-dimensional Flows	10
2.1.7	Spectral Methods on Unstructured Grids	11
2.1.8	A Stable Penalty Method for the Compressible Navier-Stokes Equations	12
2.1.9	A Fast Tau-method for Inverting Rational Variable Coefficient Operators in Bounded Domains	13
2.1.10	Acoustic Eigenmodes in Cylindrical Systems with Non-Uniform Axial Mean Flow	14
2.1.11	A Spectral Element Method for the Stokes Problem	15
2.1.12	Accurate Determination of No-slip Solvability Constraints by Recursion Calculations	16
2.1.13	Pressure Calculation on Two-dimensional Incompressible Flows	17
2.1.14	Instability of Two-dimensional Solitons and Vortices in Defocusing Media	17
2.1.15	Higher Order Nonlinear Schrödinger Equations in Continuum Physics	18
2.1.16	Defocusing Solutions of the Hyperbolic Nonlinear Schrödinger Equation	19
2.1.17	Vortex Merger in an Inhomogeneous Plasma	20
2.1.18	Magnetic Stresses in Ideal MHD Plasmas	21
2.2	Laser Plasma Diagnostics	21
2.2.1	Introduction	21
2.2.2	A Hybrid Doppler/Time-of-flight Laser Anemometer	21
2.3	Pellet Injectors for Fusion Experiments	22
2.3.1	Introduction	22
2.3.2	Construction of Multishot Pellet Injectors for FTU, Frascati, and RFX, Padova	23
2.4	Participants in the Fusion Plasma Physics Work	25
2.5	Publications and Educational Activities	26
2.5.1	Publications	26
2.5.2	Unpublished Contributions	27
3	Work in Fusion Technology	30
3.1	Irradiation Effects	30
3.1.1	Accumulation of Irradiation-induced Defects in OFHC-copper Irradiated with 3 MeV Protons	30

3.1.2	Effect of Neutron Irradiation on Microstructural Evolution and Mechanical Properties of TZM and Mo-5% Re Alloys	32
3.1.3	Temperature and Dose Dependencies of Microstructure and Hardness of Neutron Irradiated Copper	34
3.1.4	Effects of Neutron Irradiation on Microstructure and Tensile Properties of Copper Alloys	37
3.1.5	Low Cycle Fatigue Behaviour of a Cu-Cr-Zr Alloy at Room Temperature	40
3.1.6	Cascade-induced Source Hardening	42
3.1.7	Stochastic Annealing Simulation of Free Defect Production in Irradiated Metals	44
3.1.8	Helium Implanted Copper: Correlation Between TEM and Positron Annihilation Data	45
3.2	Water Radiolysis under ITER Conditions	47
3.2.1	ITER CTA Task T50: Primary Water Loop Technology	47
3.3	Participants in the Fusion Technology Work	48
3.4	Publications and Conference Contributions	49
3.4.1	Publications	49
3.4.2	Conference Contributions	49

1 Preface

The activities in the Research Unit cover two main areas:

A) Work in fusion plasma physics which includes

- *Nonlinear dynamics of fusion plasmas*
This research area is concerned with theoretical and numerical investigations of the nonlinear evolution of instabilities in magnetized plasmas and the associated turbulent transport. The emphasis in these investigations is on studies of the formation and the dynamical behavior of nonlinear, coherent structures and the influence of these structures on the total plasma flow. In order to perform detailed simulations of these processes, numerical codes based on highly accurate spectral methods have been developed.
- *New laser diagnostics for fusion plasmas*
Development has been performed of a hybrid Doppler/time-of-flight laser anemometer with increased spatial resolution for studies of turbulent density fluctuations in fusion plasmas.
- *Pellet handling, acceleration, and injection*
Pellet injectors which can inject frozen fuel pellets into fusion plasmas have been developed over the last years. Risø has offered to build injectors for fusion laboratories on commercial terms. During 1994 work was performed on two systems. One was installed at FTU in Frascati. The other system is for RFX in Padova and was made ready for shipment by the end of the year.

B) Work in fusion technology which includes

- *Work on irradiation effects in materials*
- *Work on water radiolysis under ITER conditions*

2 Work in Fusion Plasma Physics

2.1 Nonlinear Dynamics of Fusion Plasmas

2.1.1 Introduction

The research activities in this area are carried out in the Continuum Physics Section of the Optics and Fluid Dynamics Department. A unifying theme for this research is studies of nonlinear dynamical processes associated with 'self-organization', 'localization' and 'collapse'. These are fundamental phenomena which show up in an increasing number of different physical systems. Despite the apparent differences in the media in which the phenomena are observed, the generic properties of the nonlinear processes are very similar. Thus, strong vortical structures (coherent structures) with similar properties are found in drift wave turbulence in the exterior regions of magnetically confined plasmas and in the atmospheres and oceans of rotating planets. Also, the spontaneous formation of regular structures and patterns has many common features in magnetized plasmas, rotating fluids, and nonlinear optical media.

Although the emphasis of the research in the Continuum Physics Section is on theoretical and numerical investigations of nonlinear plasma dynamics, these investigations are strongly supported by experimental studies carried out in rotating liquids and in nonlinear optical media. The experimental studies allow detailed verification of the theoretical and numerical models and give rise to the formulation of new problems for theoretical and numerical investigation. Most of these experimental investigations have close plasma analogies, but they are conducted entirely outside the Fusion Research Unit. A complete listing of all the research activities in the Continuum Physics Section for 1994 can be found in the Optics and Fluid Dynamics Department Annual Progress Report for 1994 (Risø-R-793) or on the Internet under the Optics and Fluid Department home page at Risø National Laboratory (<http://www.risoe.dk>).

A major part of the studies in nonlinear plasma dynamics is connected to numerical simulations. In these studies, traditional methods in computational fluid dynamics (such as finite-difference, finite-element, and finite-volume methods) are not adequate to resolve essential details of the flow evolution. Several new codes have already been developed based on 'spectral methods' that have superior accuracy properties as compared with the traditional methods. These 'first generation' spectral codes are being used in our studies of fundamental nonlinear phenomena, but they are limited to simple geometries such as an infinite periodic array, a periodic channel, or an annulus. In order to be useful for numerical studies of plasma dynamics of more practical relevance, the algorithms need major development. This process involves employing new ideas from applied mathematics and numerical analysis. In 1994, several major steps were taken in this direction in close collaboration with research groups working with applied mathematics at American universities. These steps include the development of a multidomain, spectral algorithm employing a new method of imposing boundary conditions for compressible flows, a new algorithm for pressure calculation in incompressible flows, and a new method for accurate computation of incompressible flows in double bounded domains. All these schemes have in common that they have enhanced the accuracy of the computations significantly with very little, if any, extra cost of computer time. These methods need further development for computations of flows in three-dimensional regions with complex geometries.

2.1.2 Coherent Structures and Transport in Drift-wave Turbulence

(P.K. Michelsen, A.H. Nielsen, T. Sunn Pedersen, and J. Juul Rasmussen)

Large-scale coherent vortex structures may be created spontaneously by self-organization processes in two-dimensional turbulent flows and play a dominant role in connection with transport of materials in such flows. In magnetized plasmas it has appeared that low frequency electrostatic fluctuations, propagating in a plane perpendicular to the magnetic field, is of great importance to the plasma transport perpendicular to the magnetic field. Such systems are expected to be well described by a two-dimensional approximation. Conventional theories presume that drift wave turbulence is well described by quasi-linear coupling, i.e., a weak coupling between the relevant Fourier modes. However, recent experimental results have indicated the presence of quasi-coherent density and potential structures. Difficulties in developing an approximate edge transport model may be due to oversimplifications which exclude the existence of coherent structures.

A simplified two-dimensional two-field model for drift wave turbulence which couples the fluctuations in the plasma density to those of the plasma potential¹⁾ is investigated analytically and numerically. The system is characterized by three parameters: two viscous damping coefficients and a parameter that determines the degree of adiabatic electron response. The system is studied in the limit of small viscous damping, where the dynamic depends primarily on the adiabaticity parameter. Especially, we investigate structure formation and its relation to transport in drift wave systems.

1) Koniges, A.E., Crotinger, J.A., and Diamond, P.H. (1992). *Phys. Fluids B4*, 2785-2793.

2.1.3 Investigations of η_i -vortices and Turbulence

(J.P. Lynov, P.K. Michelsen, and J. Juul Rasmussen)

The stability and evolution of perturbed dipolar vortex solutions to a simplified two-dimensional model for the η_i -modes are investigated numerically.

Recently, it has been suggested and indicated from numerical simulations that monopolar and dipolar vortical structures could have strong influence on the dynamics of electrostatic plasma turbulence and on the associated transport in particular. Particles will not solely be transported by small-scale displacements as in diffusion-like processes, but may be trapped by coherent vortices and convected over distances much larger than the vortex scale size. High resolution simulations of, e.g., η_i -turbulence have shown that coherent vortices may develop spontaneously. These had a dominating influence on the evolution of the turbulence, and the associated anomalous transport was found to be significantly reduced as compared with the predictions from quasilinear theory. The existence of coherent vortices in two-dimensional plasma turbulence and their importance to the cross-field particle transport have also been demonstrated experimentally.

Analytical and numerical investigations have recently revealed the existence of steadily propagating monopole vortex solutions to the η_i -mode equations. These vortices propagated at velocities outside the phase velocity regime of linear waves. Even in the regime of linearly unstable waves, monopolar vortices were found to propagate and keep their identity for several times their internal turnaround time. Also dipolar vortical structures for the η_i -modes have been found and expressed analytically for simplified η_i -mode model equations. These are only exact solutions when they propagate perpendicularly to the background gradients in density and temperature.

We have performed numerical investigations of the dynamics and stability of these dipolar vortices¹⁾. In particular, we have investigated the evolution of dipoles that are initially tilted with respect to their preferred direction of propagation. The results show that the gross properties of tilted η_i -dipoles are similar to those of tilted drift wave dipoles governed by the Hasegawa-Mima equation. When the tilted dipole propagates opposite to the propagation direction of linear waves, its trajectory is gently oscillatory and the dipole keeps its structure. When it is initially propagating in the same direction as the linear waves, it starts a cycloid motion and tends to break up. Finally, we have studied the evolution of cases where the initial condition is set up in k -space with each k -mode chosen randomly in amplitude and phase.

1) Lynov, J.P., Michelsen, P.K., and Rasmussen, J. *Juul. Investigations of η_i -Vortices*, In: *Proceedings of the 1994 International Conference on Plasma Physics 2*, Foz do Iguaçu, Brazil, 31 Oct. - 4 Nov. 1994, 91.

2.1.4 Self-organization in Two-dimensional Circular Shear Layers

(K. Bergeron*, E.A. Contsias*, J.P. Lynov, and A.H. Nielsen (*University of New Mexico, USA))

Experiments in forced circular shear layers performed in both magnetized plasmas^{1,2)} and rotating fluids³⁾ reveal qualitatively similar bifurcation cascades involving states of circular vortex arrangements of varying complexity. These self-organized states have strong influence on the transport properties of the system, a problem that is relevant to fusion experiments as well as to large-scale geophysical flows. We have performed both numerical and asymptotic studies of the Navier-Stokes equations with external forcing in an annular geometry that closely reproduce the experimental observations.

While stable to radially symmetric perturbations at any value of the Reynolds number Re , the steady flow becomes unstable to azimuthal perturbations at a critical value Re_c . There ensues a braid-like arrangement of vortices straddling the forcing region and rotating at constant angular velocity. As Re is increased, these vortices grow like $(Re - Re_c)^{1/2}$ and eventually undergo a symmetry breaking transition to a new arrangement of fewer vortices. These transitions are accompanied by clear decreases in both energy and enstrophy of the whole system, as seen in Fig. 1. Further transitions can be observed as well as superpositions of various azimuthal modes with nontrivial temporal behavior. Linear stability analysis was performed to predict the first transition, and its results were found to be in close agreement with direct simulations of the flow as well as with experimental observations.

1) Pécseli, H.L., Contsias, E.A., Huld, T., Lynov, J.P., Nielsen, A.H., and Juul Rasmussen, J. (1992). *Plasma Phys. Contr. Fusion* **34**, 2065-2070.

2) Perrung, A.J. and Fajans, J. (1993). *Phys. Fluids A* **5**, 493-499.

3) Chomaz, J.M., Rabaut, M., Basdevant, C., and Couder, Y. (1988). *J. Fluid Mech.* **187**, 115-140.

2.1.5 The Temporal Evolution of the Lamb Dipole

(A.H. Nielsen, J. Juul Rasmussen, and M.R. Schmidt)

We consider the two-dimensional, unforced, incompressible Navier-Stokes equations in an unbounded domain expressed in the vorticity-stream function formulation:

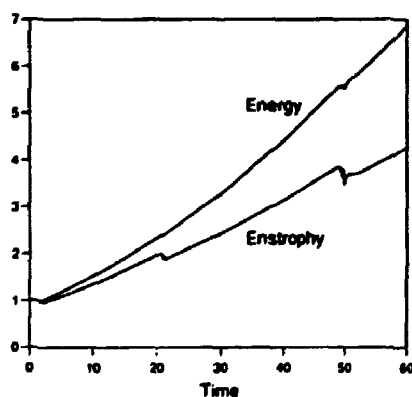
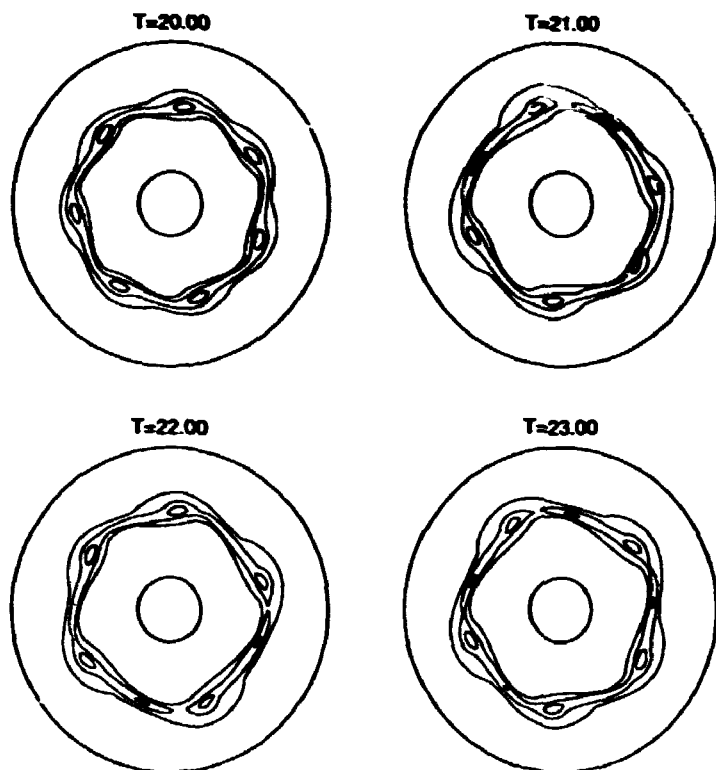


Figure 1. Symmetry breaking bifurcation during gradual speedup. The upper part shows the vorticity field during the transition from mode 7 to 5. The lower part shows the evolution of total energy and enstrophy during the whole speedup phase. The jumps mark the transitions from mode 7 to 5 and from mode 5 to 4.

$$\begin{aligned} \frac{\partial \omega}{\partial t} + [\omega, \psi] &= \nu \nabla^2 \omega, \\ \nabla^2 \psi &= -\omega, \end{aligned} \quad (1)$$

where $\omega \equiv (\nabla \times \vec{v}) \cdot \hat{z}$ is the scalar vorticity, ψ is the stream function ($\nabla \psi \times \hat{z} \equiv \vec{v}$), and ν is the viscosity. Stationary solutions to Eq. 1 in the absence of viscosity ($\nu = 0$) require that the Jacobian $[\omega, \psi]$ is equal to zero which means that there is a functional relation between the vorticity and stream function, $\omega = f(\psi)$. The most simple dipolar solution with distributed vorticity, and the only one which can be found analytically, is where this function is a linear function: $\omega = \lambda^2 \psi$ inside a circular separatrix and zero outside. This is the well known Lamb dipolar

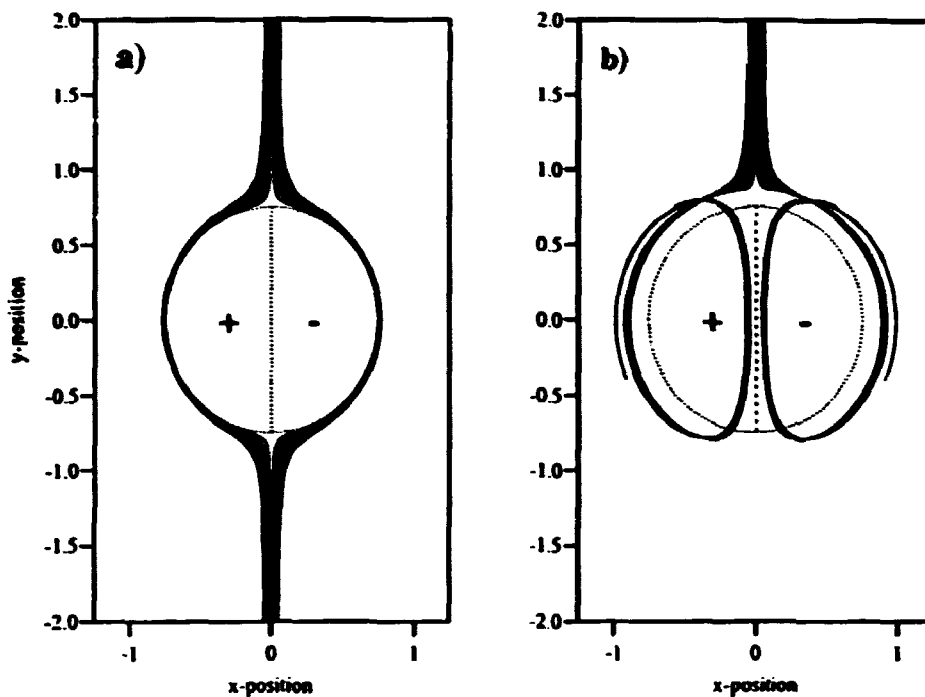


Figure 2. Figure 1. Particle trajectories in the flow field from a Lamb dipole plotted in the frame following the Lamb dipole. The particles were released in the flow field at $y = 2.0$ and in the range $x \in (-0.05; 0.05)$. Figure (a) is for no viscosity while Figure (b) is with high viscosity. The dashed line denotes the separatrix at $T = 0$.

and has the form:

$$\omega = \begin{cases} \frac{2\lambda U_0}{J_0(\lambda R_0)} J_1(\lambda r) & r \leq R_0 \\ 0 & r > R_0, \end{cases} \quad (2)$$

where U_0 and R_0 are the speed and radius of the dipole. Please note that for this solution ψ , v_θ , ω , and $\nabla^{2n}\omega$ are all continuous across the separatrix while $\nabla^{2n+1}\omega$ is discontinuous. If we inserted the solution Eq. 2 into Eq. 1, we would end up with a solution of the form: $\omega(\vec{x}, t) = \omega_0(\vec{x}) \exp(-\nu\lambda^2 t)$ which apparently shows that the Lamb dipole is stable also in the viscous case, in the sense that only its amplitude and thereby its speed will decrease, while it will keep its form. But as the solution is not differentiable at the separatrix, the effect of the viscosity is enhanced at the separatrix and tends to smear out the discontinuity in the higher derivatives of ω . A result of this is that the whole structure will expand and since the flow is incompressible, it will trap fluid from outside of the original separatrix. This can be seen in Fig. 2 where we have inserted passive particles in front of the dipole and follow their trajectories while they are convected by the dipole. In Fig. 2a we are only solving the Euler limit of Eq. 1, i.e. no viscosity, and here all the particles are moving past the structures. In Fig. 2b we see the effect of the viscosity as all the particles will become trapped as the structure expands.

2.1.6 Formation of Dipolar Vortices by Self-organization in Two-dimensional Flows

(A.H. Nielsen, J. Juul Rasmussen, and M.R. Schmidt)

The formation of dipolar vortices from localized forcing in a two-dimensional flow is investigated theoretically and by direct numerical solutions of the two-dimensional Navier-Stokes equations.

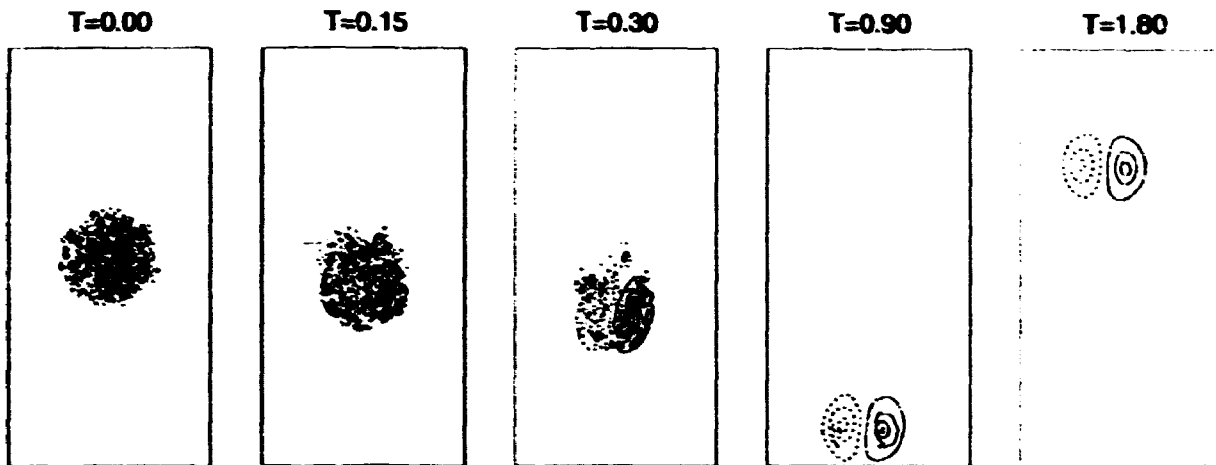


Figure 3. Evolution of a turbulent patch with initial linear momentum into a dipolar structure. The parameters are $k_0 = 20$, $\Delta = 10$, and $r_0 = 0.20$. Initially, $E = 0.314$, $W = 162$, and $P_y = 0.34$. The resolution is $N_x = N_y = 128$.

When the initial condition consists of two nearby vortices with Gaussian stream function and opposite vorticity, we observe the formation of a Lamb-type dipolar vortex, characterized by a near linear functional relationship between the stream function and the vorticity (see section 3.3.6). For distances between the centers of the initial vortices larger than a critical value measured in terms of the radii of the initial vortices, no dipolar vortex is formed. These results compare qualitatively with experimental results of dipole vortex generation in stratified fluids by van Heijst and coworkers at Eindhoven University of Technology¹). A detailed quantitative comparison is in progress.

We have also investigated the formation of dipolar vortices by self-organization of a localized turbulent patch. The patch is characterized by its energy and enstrophy and has a net linear momentum, but no net circulation. It is constructed from fluctuations with random phases and an isotropic energy spectrum, $\propto \exp(-(k - k_0)^2/\Delta^2)$; the localization of the patch is provided by multiplying this wave field by $\exp(-r^4/r_0^4)$ in configuration space, after a sinusoidal in x has been added to provide a finite linear momentum, P_y , in the y -direction. The resulting development is shown in Fig. 3. We observe a clear self-organization of the patch into a propagating dipolar structure. This development is qualitatively described as a self-organization in a viscid flow. Using the fact that the enstrophy, W , decays faster than the energy, E , we have looked for solutions that minimize W under the constraint of a fixed E and a fixed linear momentum following the idea of Leith²).

1) Flor, J.B. and van Heijst, G.J.F. (1994). *J. Fluid Mech.* **279**, 101-133.

2) Leith, C.E. (1984). *Phys. Fluids* **27**, 1388-1395.

2.1.7 Spectral Methods on Unstructured Grids

(J.S. Hesthaven, M. Carpenter (ICASE/NASA Langley Research Center, USA), and D. Gottlieb (Division of Applied Mathematics, Brown University, USA))

Traditionally, spectral methods require interpolation at the nodes of a gauss type quadrature formula. Thus, the mesh points are predetermined and inflexible. In particular the distribution of grid points is denser in the neighborhood of the boundaries which leads to considerable difficulties, even in one dimension, since

for many problems the information is given in points different from those required by the spectral method. This fact manifests itself more severely when dealing with multidimensional problems and seems to limit the applicability of spectral methods to simple domains. In two dimensions one can easily apply spectral methods to rectangular domains but the extension to other domains is not trivial.

A novel approach to overcome this limitation is to construct spectral methods from first principle. The unknown function is approximated by a general Lagrange polynomial from which differentiation operators are also obtained.

The key idea in the unstructured spectral methods is that an equation does not have to be satisfied at the same points as the derivatives are evaluated. For example, the derivative can be carried out by Lagrange interpolation at any particular point whereas the equation is satisfied in a Galerkin-, tau-, or by collocation-sense at a different set of points - 'ghost points'.

In spectral methods on unstructured grids, the boundary conditions are applied through a penalty method. This allows us to prove asymptotic stability of the methods. The accuracy of the scheme is obtained by choosing the penalty function correctly, thus allowing for proof of equivalence with the well known Galerkin-, tau-, or collocation formulations of Legendre methods.

Hence, this scheme enables us to apply spectral methods in circumstances where the grid points are not nodes of some gauss quadrature formula. Although the theoretical framework allows for multidimensional approaches by employing flux splitting, spectral methods on unstructured grids have only been thoroughly tested for one-dimensional hyperbolic problems. We are presently working on developing this approach to allow for solving problems in triangular domains. A successful implementation of such a scheme will allow us to perform spectral calculations of problems in complex domains by triangulation, similar to the approach followed for traditional low-order finite-element methods, and with similar geometric flexibility.

2.1.8 A Stable Penalty Method for the Compressible Navier-Stokes Equations

(J.S. Hesthaven and D. Gottlieb (Division of Applied Mathematics, Brown University, USA))

When addressing wave-dominated, dissipative problems, one is often forced to introduce an artificial boundary for computational reasons, e.g. for simulating open boundaries and when applying a multidomain technique. This introduces the well known problem of specifying appropriate boundary conditions at the artificial boundary. For pure γ hyperbolic problems, it is well known that enforcing these boundary conditions through the characteristic variables leads to a stable approximation. However, for dissipative wave problems the procedure is considerably more complicated.

We have developed a unified approach for dealing with open boundaries and sub-domain boundaries when performing simulations of the three-dimensional, compressible Navier-Stokes equation in conservation form. The scheme converges uniformly to the singular limit of vanishing viscosity and, hence, is also valid for the compressible Euler equation.

In the development of the scheme, we apply the energy method to the linearized, constant coefficient version of the continuous problem to obtain energy inequalities that bound the temporal growth of the solutions to the initial-boundary value problem. This approach allows us to derive a novel set of boundary conditions of the Robin type¹⁾ which ensure the complete problem to be well-posed. This result is obtained for the Navier-Stokes equations given in general curvilinear coordinates.

It has traditionally been found difficult to apply boundary conditions of the Robin type when doing pseudospectral simulations of nonlinear equations. We have shown how it is possible to implement the boundary conditions as a penalty term which allows for enforcing open boundary/patching conditions of a very general type. An attractive feature of the penalty method is that one may prove asymptotic stability of the semidiscrete scheme, thus gaining confidence in the computed results when addressing unsteady problems where long time integration is required.

A multidomain scheme, where the patching of subdomains is based on a penalty method, is strictly local in space, thus making it well suited for implementation on contemporary, parallel computer architectures with distributed memory²⁾.

The scheme has been successfully implemented to obtain multidomain solutions of one- and two-dimensional compressible, viscous flows with open boundaries. Examples include steady, transonic quasi-one-dimensional viscous nozzle flow (see Fig. 4) and unsteady flow around an infinitely long cylinder.

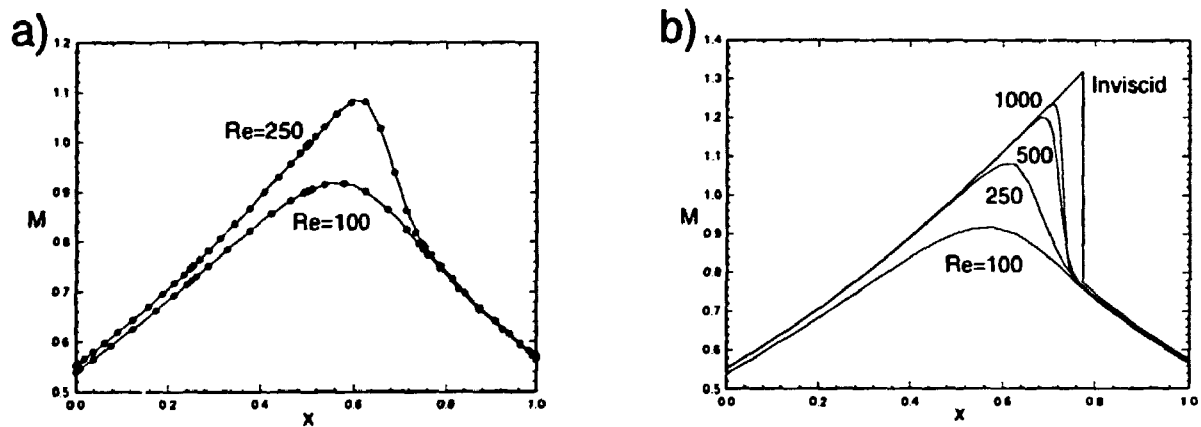


Figure 4. (a) Steady state Mach number profile for viscous, compressible flow through a Laval nozzle at low Reynolds numbers. The full lines illustrate one-domain solutions and the dots illustrate the corresponding four-domain solutions. (b) Steady state Mach number profile for viscous, compressible flow through a Laval nozzle at increasing Reynolds number compared with the inviscid analytic solution. All viscous solutions are obtained as five-domain solutions. For more details see ²⁾.

Work is now in progress to develop the software further in order to allow for addressing compressible viscous flow problems in complex geometries in two and three spatial dimensions.

1) Hesthaven, J.S. and Gottlieb, D., A Stable Penalty Method for the Compressible Navier-Stokes Equations. I. Open Boundary Conditions, SIAM J. Sci. Comp. - accepted for publication.

2) Hesthaven, J.S., A Stable Penalty Method for the Compressible Navier-Stokes Equations. II. One-dimensional Domain Decomposition Schemes, SIAM J. Sci. Comp. - submitted for publication.

2.1.9 A Fast Tau-method for Inverting Rational Variable Coefficient Operators in Bounded Domains

(J.S. Hesthaven, E.A. Coutsias¹, and D. Torres¹ (¹ Department of Mathematics and Statistics, University of New Mexico, USA))

Accurate solution of ordinary and partial differential equations with variable coefficients is of significant importance in all areas of the sciences. Traditionally, such problems are solved by using a finite difference approach in space and/or time. This results in a scheme of low to moderate order, with the error decreasing only as an algebraic function of the grid size in space and/or time. This is true even when applying spectral methods in space for solving time-dependent problems, where the traditional approach is to use some finite difference type integration in time.

The use of spectral methods in bounded geometries for problems where operators need to be inverted has in the past been restricted to only a few special cases, the reason being that the traditional formulation leads to full, nonsymmetric linear problems that are expensive and difficult to solve accurately. We have developed a novel approach, using invertible spectral operators, which results in extremely sparse linear problems; in the simplest case (a two-dimensional linear problem with constant coefficients) a tridiagonal block structure which may be solved either by special purpose direct solvers or by iterative methods, e.g. the method of quasiminimal residuals (QMRs). In our first implementation, the boundary conditions are applied as tau conditions. However, an attractive alternative is to split the solution into its homogeneous and particular part. The former part is then expanded in a basis found as the null-space of the operator, whereas the latter part is approximated by an expansion of an appropriate complete orthogonal basis, e.g. classical orthogonal polynomials, Gegenbauer polynomials, or hypergeometric functions. In this way we obtain that the treatment of the boundary conditions can be done in a numerically stable and efficient way.

The developed algorithm allows for dealing with problems with rational, variable coefficients, be the problem time-dependent or not. We see the future use of this algorithm in two main areas. The scheme allows for performing spectral time integration of ordinary and partial variable coefficient differential equations, thus obtaining schemes with uniform accuracy in time and space. The success of this approach has been confirmed by numerical experiments, where we have been able to obtain spatiotemporal errors of machine accuracy, the wave equation, and advection diffusion problems, hence establishing the method.

An alternative use of the approach is to develop accurate and fast solvers for elliptic problems, which is of significant importance in, e.g., fluid dynamics. By splitting the solution, as described above, we obtain separation of the interior and boundary part of the solution. The use of this approach allows for developing highly accurate and efficient multidomain solvers for elliptic problems, thus enabling us to design a novel multidomain algorithm for solving, e.g., the incompressible Navier-Stokes equations in complex geometries. This aspect is presently being pursued.

2.1.10 Acoustic Eigenmodes in Cylindrical Systems with Non-Uniform Axial Mean Flow

(J.S. Hesthaven, D. Gottlieb (Division of Applied Mathematics, Brown University, USA), and K. Kousen (United Technologies Research Center, East Hartford, USA))

Eigenvalue problems appear naturally in many areas of plasma physics and the development of schemes for accurately solving such problems are thus of significant importance. In particular, linear stability analysis leads to linear and non-linear eigenvalue problems for determining critical values at which the plasma flow becomes temporally or spatially unstable. To assess the accuracy of pseudospectral methods for solving such problems we have considered a non-trivial compressible

flow in a cylindrical system with a non-uniform mean flow.

Unlike their uniform counterparts, the linearized Euler equations for unsteady acoustic waves in non-uniform mean flows take the form of variable coefficient differential equations, for which no analytic solution is known. However, knowledge about the modal families that may exist under such circumstances is important as they act as the means of communication between various regions of the flow and coupled acoustic elements. Knowledge about the modal families may also be applied to construct a complete basis set for physically realistic, three-dimensional, far-field boundary conditions for unsteady direct simulation of this type of problems.

We have performed a spatial stability analysis of acoustic waves in cylindrical systems. The linearized, isentropic Euler equations for cylindrical and annular systems with mean axial shear and rotation are obtained by assuming an exponential form of the axial, azimuthal and temporal component. This results in a generalized eigenvalue problem, the solution of which yields the axial wave numbers and radial acoustic eigenmodes of the unsteady problem.

In order to solve the eigenvalue problem solution with sufficient accuracy we applied a pseudospectral Chebyshev method for spatial discretization and solved the resulting complex matrix-pencil using the QZ-algorithm.

This approach allowed us to identify a new family of eigenmodes with a continuous eigenvalue-spectrum related to the non-uniform mean flow. These modes are found to co-exist with the discrete modes known from previous analysis of the problem with uniform mean flow. Comparing with the analytic solution for uniform mean flow clearly establishes the high accuracy obtainable with this scheme.

The results found through this non-trivial test problem clearly illustrates the usefulness of pseudospectral methods for solving non-linear, variable coefficient eigenvalue problems to high accuracy with the additional advantage that eigenvalues and eigenvectors are obtained simultaneously. As such, the method provides a very general tool for studying stability problems in many areas of plasma physics.

2.1.11 A Spectral Element Method for the Stokes Problem

(B. Gervang and V.A. Barker (Technical University of Denmark))

We describe a spectral element method for solving the two-dimensional stationary Stokes problem based on the Galerkin technique and equal-order discrete subspaces for velocity and pressure. As shown by Bernardi, Canuto, and Maday¹⁾, this approach produces seven spurious pressure modes in addition to the basis hydrostatic pressure mode and, consequently, the symmetric indefinite coefficient matrix has a rank deficiency of 8. A well-known cure for this is to reduce the order of the discrete pressure subspace.

In this study we examine the consequences of maintaining the equal-order condition and working with the singular system. This procedure is facilitated by knowledge of the null-space of the matrix. The basic steps are the filtering of the right-hand side vector to obtain a consistent system, the solving of this system numerically, and the filtering of the computed pressure to remove the spurious modes.

We make an empirical study of the accuracy of the method and compare it with theory. For certain ranges of computation, the results obtained compare favorably with those published elsewhere based on unequal-order subspaces for velocity and pressure.

1) Bernardi, C., Canuto, C., and Maday, Y. (1986). C.R. Acad. Sci. Paris 303 series I, 971-974.

2.1.12 Accurate Determination of No-slip Solvability Constraints by Recursion Calculations

(E.A. Coutsias (University of New Mexico, USA) and J.P. Lynov)

When calculating solutions to the incompressible Navier-Stokes equations in two dimensions, it is advantageous to work in the vorticity-stream function formulation. Compared with the primitive variable approach, described by velocity and pressure, the vorticity-stream function formulation reduces the number of scalar dynamic equations from two to one, it eliminates the pressure from the calculations, and the incompressibility condition, $\nabla \cdot \mathbf{u} = 0$, is satisfied by construction. However, no-slip boundary conditions leave the Poisson equation, relating the vorticity to the stream function, overdetermined.

We have previously shown¹⁾ how this overdeterminacy can be resolved by imposing solvability constraints on the vorticity field. In particular, we have shown how these constraints can be implemented in spectral algorithms for two-dimensional flows in geometries that are bounded in one direction and periodic in the other, i.e. periodic channel, annulus, and disk geometries. In these cases, the fields are expanded in Fourier-Chebyshev series. For each Fourier mode, the solvability constraints lead to a set of two linear equations for the Chebyshev expansion coefficients of the vorticity field. The constants in these two equations are expressed analytically in terms of Dirichlet Green's functions for the Poisson equation, and they can be determined numerically in a preprocessing step.

It is obvious that precise determination of these solvability constants is essential to the overall accuracy of the calculations. In our previous work, these constants were determined by direct numerical solution of a large number of Poisson equations, one for each combination of Fourier and Chebyshev mode. The numerical values for the constants converge quickly with increasing mode number truncation. However, we were missing a good estimate of the error in the calculations.

In order to resolve this question, we have carried out a more detailed investigation. Analytical expressions for the required Green's functions in the different geometries (channel, annulus, and disk) were obtained, and after some simple calculations only Chebyshev expansions of analytical functions remained. Unfortunately, these expansions converge extremely slowly (quadratically) with increasing mode number, leaving this approach useless.

A different approach was found after deriving a three-term recursion relation between successive solvability constants for increasing Chebyshev mode number and fixed Fourier mode number. Although a direct forward solution following this recursion relation is impossible due to numerical instability, a careful treatment of the three-term difference equation yielded very good results. As a first step in this treatment, both the dominant and the minimal solution to the homogeneous problem²⁾ are found following a forward and a backward recursion, respectively. Based on these homogeneous solutions, a full solution to the inhomogeneous problem was constructed following the method of variation of constants. The solutions converged rapidly with increasing mode truncation to within machine-order accuracy, and direct error checks show results better than 10^{-13} . Fortunately, comparisons between our new values for the solvability constants and our older ones determined by numerical solution of the many Poisson equations show excellent agreement.

1) Coutsias, E.A. and Lynov, J.P. (1991). *Physica D* **51**, 482-497.

2) Gautschi, W. (1967). *SIAM Review* **9**, 24-82.

2.1.13 Pressure Calculation of Two-dimensional Incompressible Flows

(E.A. Coutsias (University of New Mexico, USA), J.S. Hesthaven, and J.P. Lynov)

The accurate calculation of the pressure field in simulations of incompressible flows is of significant importance to applications since it is easily measurable. Although the pressure field evolution must be followed as part of the solution of the problem in the primitive variable formulation, the pressure in the vorticity-stream function formulation of two-dimensional flows is eliminated and, thus, a special treatment is required.

In the velocity-pressure formulation, the pressure is calculated by taking the divergence of the momentum equation and enforcing incompressibility. This approach results in a Poisson equation for the pressure. Unfortunately, it is easy to show that this problem is overdetermined due to the existence of too many boundary conditions. Several approaches have been proposed to resolve this problem, but they all rely on solving a large linear system at each time step and, hence, are very time consuming.

We have followed a different approach which allows for a self-consistent calculation of the pressure distribution from the instantaneous vorticity field in a postprocessing stage.

In the development of the algorithm, special attention was given to accuracy issues by minimizing the maximum order of derivatives. As a result, only first-order derivatives enter in the calculation. This is of significant importance to very high resolution spectral simulations of flows.

We have successfully implemented the scheme for a planar channel flow at high Reynolds numbers and have calculated the pressure field with a global error of $\mathcal{O}(10^{-7})$. This new approach supplies important new information about the relation between the pressure distribution and the vorticity generation at no-slip walls. An example of the vorticity and pressure fields calculated in a high resolution simulation with 1,024 Fourier modes and 512 Chebyshev modes is shown in Fig. 5.

2.1.14 Instability of Two-dimensional Solitons and Vortices in Defocusing Media

(E.A. Kuznetsov (Landau Institute for Theoretical Physics, Moscow, Russia) and J. Juul Rasmussen)

The stability of two-dimensional soliton and vortex solutions to the nonlinear Schrödinger equation (NLSE) with repulsion is considered. This equation which reads:

$$i\psi_t + \frac{1}{2}\nabla^2\psi + (1 - |\psi|^2)\psi = 0 \quad (1)$$

has several important applications in nonlinear optics and plasma physics. For these cases two-dimensional soliton and topological vortex solutions have been investigated both theoretically and numerically.

We have investigated the stability of the whole family of these two-dimensional solutions with respect to three-dimensional perturbations in the framework of Eq. (1). We found that the structures are in general unstable with respect to long wavelength symmetric perturbations, while they appear to be stable with respect to antisymmetric perturbations. In the limit where these soliton solutions have large velocities ($v \rightarrow C_s$, where C_s is the "sound" velocity, the minimum phase

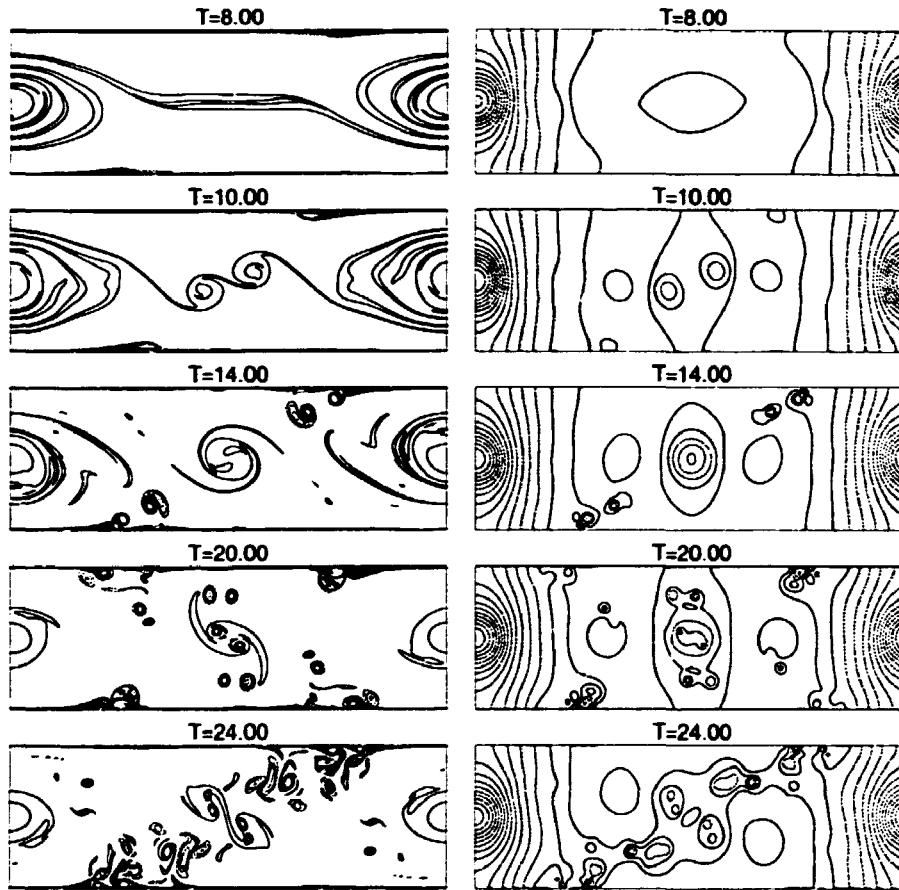


Figure 5. Vorticity (left) and pressure (right) in a plane, incompressible Couette flow at $Re = 40,000$. The full contours show positive values, and the dashed contours negative values.

velocity of linear waves), the instability is analogous to the instability of one-dimensional acoustic solitons in a medium with positive dispersion as described by the Kadomtsev-Petviashvili equation. For smaller velocities the structure appears as a dipolar vortex and here the instability becomes similar to the so-called Crow instability of two vortex filaments with opposite circulations in hydrodynamics as described in terms of the Euler equations. It is conjectured that the nonlinear evolution of this instability will lead to a reconnection of the vortex filaments and to the formation of vortex rings.

2.1.15 Higher Order Nonlinear Schrödinger Equations in Continuum Physics

(J. Wyller (Narvik Institute of Technology, Norway), T. Flå (University of Tromsø, Norway), and J. Juul Rasmussen)

Under a slowly varying amplitude assumption, the modulation of small, but finite amplitude wave trains in one dimension is described by a Schrödinger type of equation with a cubic nonlinearity. In magnetized plasmas, for example, the nonlinearity describes the change in the plasma density with the amplitude of the electromagnetic wave. The higher order nonlinear Schrödinger equation (HNLS-equation):

$$i\phi_\tau + \phi_{\xi\xi} = a_1|\phi|^2\phi + a_2|\phi|^4\phi + ia_3|\phi|^2\phi_\xi + (a_4 + ia_5)\phi(|\phi|^2)_\xi \quad (1)$$

can describe wave propagation when higher order nonlinearities are taken into account. Here a_i ($i = 1, \dots, 5$) are real coefficients and $\phi(\xi, \tau)$ represents the slowly varying amplitude, τ is the propagation coordinate and ξ the reduced time coordinate, both being normalized to true physical quantities. In this context, the nonlinear terms represent: the Kerr effect ($a_1|\phi|^2\phi$), the first-order contribution to the nonlinear saturation ($a_2|\phi|^4\phi$), the nonlinear dispersion ($ia_3|\phi|^2\phi_\xi$ and $ia_5(|\phi|^2)_\xi\phi$), and the Raman effect ($a_4(|\phi|^2)_\xi\phi$). In addition to optical phenomena, Eq. (1) with $a_4 = 0$ is a model for the so-called marginally stable modulated wave trains in different physical systems.

When $a_3 \neq 0$, Eq. (1) can be transformed to the following extended derivative nonlinear Schrödinger equation:

$$q_t + iq_{xx} + |q|^2q_x + i\gamma(|q|^2)_xq + i\sigma|q|^4q = 0 \quad (2)$$

by means of a point transformation and a subsequent gauge transformation. Here γ is proportional to a_4 and σ is a function of a_1, a_2, a_3 , and a_5 . The properties of this equation are summarized as follows:

- When $\gamma = \sigma = 0$, Eq. (2) is completely integrable and can be solved by means of the inverse scattering transform. The soliton solutions represent self-phase modulated wave packets.
- When $\gamma = 0$, Eq. (2) is a Hamiltonian system possessing three conservation laws (i.e. conservation of action, momentum, and energy). A detailed study of Eq. (2) with respect to cnoidal waves, linear and nonlinear stages of the modulational instability and recurrence has been carried out by Flå and Wyller¹⁾. The instability criterion reads $k_0 > -2\sigma q_0^2$, where k_0 and q_0 are carrier wave number and amplitude, respectively, of the plane wave solution to Eq. (2).
- When $\gamma \neq 0$, $\sigma \neq 0$, only the action density is conserved. The plane wave solutions of Eq. (2) are modulationally unstable in all regimes of the carrier wave number k_0 and amplitude q_0 . The periodic cnoidal waves, which exist in the case $\gamma = 0$, are destroyed by the Raman term $i\gamma(|q|^2)_xq$.
- Equation (2) possesses group invariant solutions of the self-similar type for all combinations of σ and γ .

1) Flå, T. and Wyller, J. (1993). *Physica Scripta* 47, 214.

2.1.16 Defocusing Solutions of the Hyperbolic Nonlinear Schrödinger Equation

(L. Bergé (Commissariat à l'Énergie Atomique, CEIV, France) and J. Juhl Rasmussen)

The elliptic/hyperbolic nonlinear Schrödinger equation

$$iu_t + u_{rr} + (d-1)u_r/r + su_{zz} + |u|^2u = 0 \quad (1)$$

is the canonical equation that governs the propagation of the envelope $u(r, z, t)$ of an almost monochromatic, weakly nonlinear packet of dispersive waves. It arises in a wide variety of contexts, such as plasma physics and nonlinear optics when the transverse (r -plane of dimension number d) distribution of a high frequency carrier wave is modulated by slow-frequency motions as the wave propagates along the longitudinal z -axis.

By means of a Lagrangian approach, $d = 1$ solutions were recently described in both situations of so-called anomalous and normal dispersions corresponding to the elliptic/hyperbolic values $s = +1$ and $s = -1$, respectively¹⁾: it was shown that when $s = +1$, an anisotropically-shaped localized structure having a negative

energy tends to collapse in a finite time with an identical contraction rate in both transverse and longitudinal directions, while in the opposite case when $s = -1$, the waveform asymptotically defocuses with a linear-in-time dilation rate. Even though these results remain in good agreement with various numerical results, the global behavior of $u(r, z, t)$ in the presence of normal dispersion has never been examined from a mathematical point of view in the past. The present work therefore consists in establishing rigorous estimates based upon some concavity arguments: they prove that the solution $u(r, z, t)$ - initially localized in space - spreads out in time for $s = -1$, at least in the following situations:

(i) In the two-dimensional case ($d = 1$); if the initial velocity of the structure defined along the z -axis is strictly positive, then the wave packet disperses along this axis in a finite time. For all other initial data, the wave surely spreads out as t tends to infinity, and the transverse size of the structure never tends to zero even when its energy is negative, unlike the $s = +1$ case;

(ii) In the three-dimensional case ($d = 2$), a positive energy wave packet also disperses in a finite time when the initial velocity of the solution is strictly positive along the longitudinal axis, and asymptotically defocuses for different initial velocities. The fate of a three-dimensional structure evolving with a negative energy in a normal dispersive medium, however, remains under investigation.

(iii) Besides, no nonzero localized stationary solution exists whatever the space dimension number d may be.

Finally, resulting from a perturbative analysis performed around the stationary ground state of Eq. (1) defined for $s = 0$ and $d = 2$, the salient difference between both cases, $s = +1$ and $s = -1$, is that a z -periodic perturbation induces a local self-concentration of the ground state mass in the first situation (which can ultimately lead to the collapse), whereas in the second situation the same mass tends to disperse along the z -axis, hereby reflecting the delocalising dynamics summarized above.

1) Bergé, L. (1994). Phys. Lett. A 189, 290-298.

2.1.17 Vortex Merger in an Inhomogeneous Plasma

(X. He (also CATS, Niels Bohr Institute, University of Copenhagen, Denmark) and J. Juul Rasmussen)

Using a probabilistic method, we present a functional critical separation distance d_c for two circular patches unequal in vorticity and radius in an inhomogeneous plasma under the assumption of low frequency, electrostatic fluctuations. These conditions are relevant to the plasma edge region in tokamaks and stellarators. We first impose two forces on the vortices: one is internal local strain $F_i = -\omega_1 R_1^2 / (\tau \delta)$, the other is external background rotation $F_e = \tau^2 f^2 / \Gamma$, where f is proportional to the background plasma density gradient. We then seek for the most likely probability of finding the two vortex centers separated over a distance r , from which the critical distance d_c is derived by using the geometrical argument and defining the merger criterion for the small vortex. We show that in the case of an identical vortex pair, a pair with the same sign vorticity as the background rotation has larger critical distances than a pair with opposite sign to the background rotation. The result supports the explanation in a numerical simulation for the anomalous vortex merger.

2.1.18 Magnetic Stresses in Ideal MHD Plasmas

(V.O. Jensen)

A comprehensive study of the advantages of using magnetic stresses for determining steady state equilibria of ideal MHD plasmas has been undertaken. The basic equations are:

$$\text{the force density equation, } \mathbf{j} \times \mathbf{B} = \nabla p \quad (1)$$

$$\text{the Maxwell equations, } \nabla \times \mathbf{B} = \mu_0 \mathbf{j} \quad \text{and } \nabla \cdot \mathbf{B} = 0. \quad (2)$$

It is shown that the resulting stresses acting on an area element, ds , in a magnetized plasma comprise:

- A shear stress, $B_{\parallel} B_{\perp} / \mu_0$, acting along the projection of the \mathbf{B} -lines on ds .
- A tensile stress, B_{\perp}^2 / μ_0 , acting perpendicular to ds .
- A compressive stress, $B^2 / 2\mu_0$, acting perpendicular to ds .
- A particle pressure, p , acting perpendicular to ds .

The stresses are used to derive and explain various properties of magnetically confined plasmas.

2.2 Laser Plasma Diagnostics

2.2.1 Introduction

Despite many years of intensive research and development towards the use of magnetically confined plasmas for the production of energy, much remains unknown about the basic physical processes inside the plasma. There is an ongoing need for the development of new diagnostic techniques that allow detailed measurements to be performed, without disturbing the plasma. Within the framework of Risø's association with EURATOM, we are developing a time-of-flight type laser anemometer for measurements of electron density fluctuations in plasmas.

2.2.2 A Hybrid Doppler/Time-of-flight Laser Anemometer

(M. Saffman, L. Lading, S.G. Hanson, T.M. Jørgensen, and R.V. Edwards (Case Western Reserve University, Cleveland, USA))

The Doppler type laser anemometer, where the velocity is found from measuring the differential Doppler shift of light scattered from a pair of crossed beams, has for many years been used for measurements of plasma turbulence. These measurements are plagued, however, by very poor spatial resolution along the beams due to the small scattering angles that are necessary for measurements of turbulence of long wavelength. In order to correct this deficiency we have proposed using a time-of-flight type configuration for plasma measurements¹⁾. The tightly focused beams of the time-of-flight anemometer result in a great improvement in the axial resolution, without sacrificing accuracy in the velocity measurement. In order to have sufficient sensitivity to measure the weak phase perturbations encountered in plasmas, it is necessary to work with a reference beam configuration. The resulting system is a hybrid combination of the Doppler and time-of-flight approaches. An interesting byproduct of this work is that the hybrid design may be superior to existing laser anemometers. An information theoretic analysis²⁾ shows that in principle it has a much lower measurement uncertainty than either the Doppler or the time-of-flight approaches.

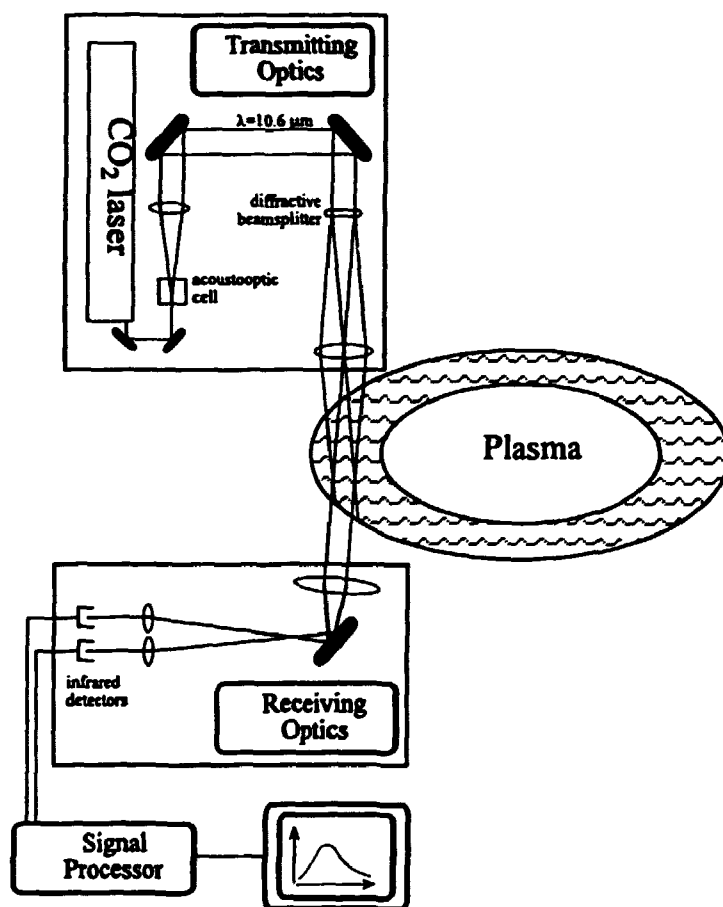


Figure 6. Generic layout of a light scattering diagnostic for measurement of plasma density fluctuations.

The generic layout of such a scattering experiment is shown in Fig. 6. An 80 W cw CO₂ laser operating at 10.6 mm is split into four beams using an acousto-optic cell together with a specially fabricated ZnSe diffractive element. The infrared detectors are liquid nitrogen cooled HgCdTe photoconductors. This system is currently being tested at Risø using a turbulent air jet. It is planned, upon successful completion of these tests, to move the system to the Wendelstein VII-A stellarator at the Max Planck Institute for Plasma Physics in Garching, for measurements on a large-scale plasma device.

- 1) Lading, L., Saffman, M., Hanson, S.G., and Edwards, R.V. "A Combined Doppler and Time-of-flight Laser Anemometer for Measurement of Density Fluctuations in Plasmas", submitted to The Journal of Atmospheric and Terrestrial Physics, June 1994.
- 2) Saffman M. and Jørgensen, T.M. "On the Optimum Spatial Code of a Laser Anemometer", submitted to Opt. Comm., December 1994.

2.3 Pellet Injectors for Fusion Experiments

2.3.1 Introduction

Injection of frozen hydrogen or deuterium pellets is an essential part of several plasma fusion experiments. Risø has developed a system for this type of pellet injection. The department has offered to build injectors for fusion experiments on commercial terms. During 1994 we have worked on two systems. One was installed

at FTU in Frascati. The other system is for RFX in Padova and was made ready for shipment by the end of the year.

2.3.2 Construction of Multishot Pellet Injectors for FTU, Frascati, and RFX, Padova

(H. Sørensen, B. Sass, K-V. Weisberg, and J. Bundgaard (Engineering and Computer Department, Risø))

The multishot pellet injector delivered to FTU in November 1993 was set up at FTU by the FTU staff in April-May 1994. It was used for injection of pellets until July when FTU was closed down for major maintenance.

The injector for RFX should have been delivered in May 1994 but the delivery was postponed to coincide with a large shutdown. It is now planned that this shutdown will take place in January-April 1995 and delivery must then take place during this period.

The two injectors are similar in design.

Eight pellets of hydrogen or deuterium are made simultaneously and fired successively. They pass through a diagnostic unit where mass and velocity are measured. They continue to the experiment through a guide tube system. They pass two large vacuum chambers where most of the driver gas is removed.

There are, however, differences that made the building and commissioning of the RFX injector more difficult. The main differences are: longer flight distance for pellets for the RFX injector before entering the experiment; larger pellets and, thus, larger gun barrel diameters; stronger cooling needed because of larger pellets; pellets of three different sizes in the RFX injector and only two in the FTU injector; for RFX pellets should be fired with time intervals around 10 ms, for FTU around 100 ms; in the torus hall the cables and tubes between the injector cubicle with instruments and the injector had to be around 12 m at RFX against 2 m at FTU.

The larger effective distance between cubicle and injector meant that the methods for change of pressurized cylinders for pellet gas had to be improved to avoid contamination of pellet gas.

The firing accuracy must then be largest for the RFX injector. In fact, the pellets must be well inside a 25 mm circle 3500 mm in front of the gun barrels.

The gun barrels are very close to each other. When pellets are fired with small time intervals, the flight of a pellet may be affected by driver gas leaving the neighbor barrel after the preceding shot. In the RFX injector the pellets are fired in the succession large-small-large-small etc. and the firing accuracy of the smaller pellets may then be affected.

The RFX injector must then fire more accurately and at the same time some of the pellets are more inaccurate. This was solved by using the same technique as in the feasibility study made earlier. Here the pellet trajectories were held together by sending the pellets through a 16 mm tube during the last part of their flight. This tube thus acted as a guide tube for some pellets. The same technique was used during test of the RFX injector. A 1,500 mm long tube of 16 mm inside diameter ending around 3,300 mm in front of the gun barrels was mounted and lined up very precisely. An optical detector was set up after this tube and connected to an electronic counter.

It is then possible to check that the same number of pellets is registered by the counter and the diagnostic unit. The pellets hit an aluminum plate of 0.3 mm thickness placed after the 16 mm tube and it is then also possible to see how much the pellets scatter.

Using this method with the aluminum plate placed 3,900 mm in front of the gun barrels, all pellets were inside a 17-20 mm circle for high and low velocity pellets of both hydrogen and deuterium.

For deuterium pellets high velocities are around 1,250-1,300 m/s and low velocities around 730-780 m/s. For hydrogen high velocities are around 1,400-1,450 m/s and low velocities around 800-900 m/s. Velocities vary from one barrel to the other. Scatter in velocity for the individual barrels is around 0.5-2.0%.

For both hydrogen and deuterium the nominal pellet sizes are $1.5 \cdot 10^{20}$, $3 \cdot 10^{20}$, and $5 \cdot 10^{20}$ atoms/pellet. There are four small pellets and two of each of the larger ones. The true pellet size for a barrel may differ up to 6-7% for the nominal one. For each barrel the standard deviation for the scatter in mass is around 2-6%.

2.4 Participants in the Fusion Plasma Physics Work

Scientific Staff

Gervang, Bo
Jensen, Vagn O.
Lading, Lars
Lynov, Jens-Peter
Michelsen, Poul K.
Nielsen, Anders H.
Rasmussen, Jens Juul
Saffman, Mark (from 1 April)
Sørensen, Hans
Weisberg, Knud-V. (until 31 October)

Ph.D. Students

Hesthaven, Jan S.
Schmidt, Michel R. (from 1 October)

Technical Staff

Astradsson, Lone
Bækmark, Lars
Michelsen, Agnete (until 30 April)
Nielsen, Mogens O.
Reier, Børge
Sass, Bjarne
Thorsen, Jess

Secretaries

Jensen, Elin
Skaarup, Bitten (from 15 December)
Toubro, Lene

Guest Scientists

Bergé, Luc, Commissariat à l'Énergie Atomique, Centre d'Études de Limeil-Valenton, France
He, Xingyu, University of Warwick, Coventry, England
Wyller, John, Narvik Institute of Technology, Norway

Short-term Visitors

Luther, G.G., University of New Mexico, Albuquerque, USA
Pécseli, H.L., University of Oslo, Norway
Scott, B.D., Max-Planck-Institut für Plasmaphysik, Garching, Germany
Sutyryn, C. G., P.P. Shirshov Institute of Oceanology, Moscow, Russia

Students Working for the Master's Degree

Pedersen, Thomas Sunn

Student Assistants

Schmidt, Michel R. (January 17-28 and September 19 - October 1)

2.5 Publications and Educational Activities

2.5.1 Publications

- Coutsias, E.A.; Bergeron, K.; Lynov, J.P.; Nielsen, A.H., Self organization in 2D circular shear layers. In: 25th AIAA plasmadynamics and lasers conference. 25. AIAA plasmadynamics and lasers conference, Colorado Springs, CO (US), 20-23 Jun 1994. (American Institute of Aeronautics and Astronautics, Washington, DC, 1994) (AIAA-94-2407) 11 p.
- Hesthaven, J.S.; Gottlieb, D., A stable penalty method for the compressible Navier-Stokes equations. I. Open boundary conditions. (Institute for Computer Applications in Science and Engineering, NASA Langley Research Center, Hampton, VA, 1994) (NASA-CR-194961; ICASE-R-94-68) 41 p.
- Karpman, V.I.; Lynov, J.P.; Michelsen, P.K.; Juul Rasmussen, J., Modulational instability evolution in two dimensions. In: 1994 International conference on plasma physics. Proceedings. Contributed papers. Vol. 2. 10. Kiev international conference on plasma theory; 10. International congress on waves and instabilities in plasmas; 6. Latin American workshop on plasma physics, Foz do Iguacu, PR (BR), 31 Oct - 4 Nov 1994. Sakanaka, P.H.; Bosco, E. Del; Alves, M.V. (eds.), (INPE/Setor de Eventos, Sao Jos dos Campos, SP, 1994) p. 71-74.
- Jensen, V.O., Alfvenbølger. Den store Danske Encyclopædi, Danmarks Nationalleksikon, vol. I, p. 249, 1994.
- Karpman, V.I.; Lynov, J.P.; Michelsen, P.K.; Juul Rasmussen, J., Modulational instability of plasma waves in two dimensions. In: Computational physics nonlinear dynamical phenomena in physical, chemical and biological systems. 3. IMACS international conference on computational physics, Lyngby (DK), 1-4 Aug 1994. Leth Christiansen, P.; Mosekilde, E. (eds.), (IMACS Secretariat, Department of Computer Science, Rutgers University, Piscataway, NJ, 1994) p. 113-118.
- Lading, L., Principles of laser anemometry. In: Optical diagnostics for flow processes. Lading, L.; Wigley, G.; Buchhave, P. (eds.), (Plenum Press, New York, 1994) p. 85-126.
- Lading, L.; Edwards, R.V.; Hanson, S., A phase screen approach to collective light scattering; Resolving temporal fluctuations. In: Seventh international symposium on applications of laser techniques to fluid mechanics. Vol. 1. 7. International symposium on applications of laser techniques to fluid mechanics, Lisbon (PT), 11-14 July 1994. (The Calouste Gulbenkian Foundation, Lisbon, 1994) p. 1.1.1-1.1.6.
- Lading, L.; Wigley, G.; Buchhave, P. (eds.), Optical diagnostics for flow processes. (Plenum Press, New York, 1994) 398 p.
- Lynov, J.P.; Coutsias, E.A.; Hesthaven, J.S., New spectral algorithms for accurate simulations of bounded flows. In: Advanced concepts and techniques in thermal modelling. Oral and poster communications extended papers. EURO THERM seminar 36, Poitiers (FR), 21-23 Sep 1994. (Laboratoire d'Etudes Thermiques, Poitiers, 1994) p. N16-N21.
- Lynov, J.P.; Hesthaven, J.S.; Juul Rasmussen, J.; Nycander, J.; Sutyryn, G.G.; Shirshov, P.P., Coherent structure in anisotropic plasmas. In: 25th AIAA plasmadynamics and lasers conference. 25. AIAA plasmadynamics and lasers conference, Colorado Springs, CO (US), 20-23 Jun 1994. (American Institute of Aeronautics and Astronautics, Washington, DC, 1994) (AIAA-94-2408) 8 p.
- Lynov, J.P.; Michelsen, P.K.; Juul Rasmussen, J., Investigations of etai-vortices. In: 1994 International conference on plasma physics. Proceedings. Contributed papers. Vol. 2. 10. Kiev international conference on plasma theory; 10. International congress on waves and instabilities in plasmas; 6. Latin American

- workshop on plasma physics, Foz do Iguacu, PR (BR), 31 Oct - 4 Nov 1994. Sakanaka, P.H.; Bosco, E. Del; Alves, M.V. (eds.), (INPE/Setor de Eventos, Sao Jos dos Campos, SP, 1994) p. 91-94.
- Nielsen, A.H.; Lynov, J.P.; Coutias, E.A.; Bergeron, K., Self organization in 2D circular shear layers. In: *Computational physics nonlinear dynamical phenomena in physical, chemical and biological systems. 3. IMACS international conference on computational physics*, Lyngby (DK), 1-4 Aug 1994. Leth Christiansen, P.; Mosekilde, E. (eds.), (IMACS Secretariat. Department of Computer Science. Rutgers University, Piscataway, NJ, 1994) p. 119-124.
- Nielsen, A.H.; Pécseli, H.L.; Juul Rasmussen, J., Experimental evidence for mode selection in turbulent plasma transport. *Europhys. Lett.* (1994) v. 27 p. 209-214.
- Raadu, M.A.; Rasmussen, J.J.; Turitsyn, S.K., Stability of small-amplitude double layers in a two-temperature plasma. *Plasma Phys. Rep.* (1993) v. 19 p. 531-536.
- Rasmussen, J. Juul; Hesthaven, J.S.; Lynov, J.P.; Nielsen, A.H.; Schmidt, M.R., Dipolar vortices in two-dimensional flows. (Invited contribution). In: *Computational physics nonlinear dynamical phenomena in physical, chemical and biological systems. 3. IMACS international conference on computational physics*, Lyngby (DK), 1-4 Aug 1994. Leth Christiansen, P.; Mosekilde, E. (eds.), (IMACS Secretariat. Department of Computer Science. Rutgers University, Piscataway, NJ, 1994) p. 1-11.
- Rasmussen, J. Juul; Stenum, B., Visualization of coherent structures. In: *Optical diagnostics for flow processes*. Lading, L.; Wigley, G.; Buchhave, P. (eds.), (Plenum Press, New York, 1994) p. 291-302.
- Rasmussen, J. Juul; Lynov, J.P.; Hesthaven, J.S.; Sutyryn, G.G., Vortex dynamics in plasmas and fluids. *Plasma Phys. Controlled Fusion* (1994) v. 36 p. B193-B202.
- Sutyryn, G.G.; Hesthaven, J.S.; Lynov, J.P.; Juul Rasmussen, J., Dynamical properties of vortical structures on the beta-plane. *J. Fluid Mech.* (1994) v. 268 p. 103-131.
- Sønderberg Petersen, L.; Jensen, V O., Drømmen om en udtømmelig energikilde er rykket nærmere virkeligheden. *Risø nyt* (1994) (no. 3) p. 10-11.
- Sønderberg Petersen, L.; Jensen, V.O., Drømmen om en udtømmelig energikilde er rykket nærmere virkeligheden. *DaFFO-nyt. Dansk Forening til Fremme af Opfindelser* (1994) v. 22 (no. 6) p. 6-11.

2.5.2 Unpublished Contributions

- Hesthaven, J.S., The penalty method for systems of hyperbolic and mixed type (invited lecture). In: *Spectral Multi-Domain Workshop*, Rayleigh, North Carolina (US), 18-21 May 1994. Unpublished.
- Hesthaven, J.S., A penalty method for problems in fluid mechanics. In: *Workshop on Spectral Methods*, The Technical University of Denmark, Lyngby (DK), 27 May 1994. Unpublished.
- Hesthaven, J.S., Penalty methods for spectral methods. Lecture at University of New Mexico, Department of Mathematics and Statistics, Albuquerque (US). Unpublished.
- Hesthaven, J.S.; Lynov, J.P.; Nielsen, A.H.; Rasmussen, J.J.; Schmidt, M.R.; Shapiro, E.G.; Turitsyn, S.K., Dynamics of nonlinear dipole vortices. *European Geophysical Society 19. general assembly*, Grenoble (FR), 25-29 Apr 1994. Unpublished. Abstract available.
- Hesthaven, J.S.; Lynov, J.P.; Nielsen, A.H.; Juul Rasmussen, J.; Schmidt, M.R., Dynamics of nonlinear dipole vortices. Danish Physical Society spring meeting,

- Odense (DK), 2-3 Jun 1994. Unpublished. Abstract available.
- Hesthaven, J.S., No-slip boundary conditions for the 2D Navier-Stokes equations in the $\omega - \psi$ formulation. Lecture at Brown University, Division of Applied Mathematics Providence, Rhode Island (US), 11 February 1994. Unpublished.
- Jensen, V.O., Fusionsplasmafysik. Forelæsningsserie. Danmarks Tekniske Universitet, Lyngby (DK), September-December 1994. Unpublished. Lecture notes available.
- Jensen, V.O., Magnetic stresses in ideal MHD. 29. Nordic plasma and gas discharge symposium, Geilo (NO), 31 Jan - 2 Feb 1994. Unpublished. Abstract available.
- Jensen, V.O., Magnetiske spændinger i statiske magnetfelter. Afdelingen for Elektrofysik. DTU, Lyngby (DK), 24 Jan 1994. Unpublished. Abstract available.
- Jensen, V.O., Fusion. Ungdommens Naturvidenskabelige Forening. UNF, København (DK), 1 Sep 1994. Unpublished. Abstract available.
- Jensen, V.O., Fusionsenergien, Fremtidens udtømmelige energikilde. Plancher vist på Danmarks Tekniske Museum under energi udstilling, juni - December 1994.
- Jensen, V.O., Fusionsenergien, fremtidens udtømmelige og miljøvenlige energikilde. Fællesseminar for VUC-centrene i København (DK), 30 november 1994. Unpublished.
- Kuznetsov, E.A.; Rasmussen, J.J., Instability of two-dimensional solitons and vortices in a defocusing media. International workshop on nonlinear Schroedinger equation: Achievements, developments, perspectives (NLS-94), Chernogolovka, Moscow Region (RU), 25 Jul - 3 Aug 1994. Unpublished. Abstract available.
- Kuznetsov, E.A.; Rasmussen, J.J.; Rypdal, K.; Turitsyn, S.K., Sharper criteria for the wave collapse. (Invited contribution). International workshop on nonlinear Schroedinger equation: Achievements, developments, perspectives (NLS-94), Chernogolovka, Moscow Region (RU), 25 Jul - 3 Aug 1994. Unpublished. Abstract available
- Lading, L.; Coherent light scattering. In: W7-X Diagnostic-Working Session, Garching (G), 3 March 1994. Unpublished.
- Lading, L.; Edwards, R.V., A phase screen approach to collective light scattering. Aussis (F), 21-24 March 1994. Unpublished.
- Lading, L.; Edwards, R.V., A phase screen approach to collective light scattering. Laser '94. Dansk Optisk Selskab. Dansk Fysisk Selskab, Odense (DK), 12-13 Apr 1994. Unpublished. Abstract available.
- Lynov, J.P.; Bergeron, K.; Coutias, E.A.; Nielsen, A.H., Evolution of circular shear layers. In: 1994 IEEE international conference on plasma science. IEEE conference record - abstracts. 1994 IEEE international conference on plasma science, Santa Fe, NM (US), 6-8 Jun 1994. (Institute of Electrical and Electronics Engineers, New York, 1994) p. 81-82.
- Lynov, J.P., Accurate Determination of no-slip solvability constraints. Department of Mathematics and Statistics, University of New Mexico, Albuquerque (US), 18 May 1994. Unpublished.
- Lynov, J.P., Full-wave calculations of the O-X mode conversion in magnetized plasmas. Department of Mathematics and Statistics, University of New Mexico, Albuquerque (US), 22 February 1994. Unpublished.
- Lynov, J.P., Two-dimensional dipole interactions with straight and curved walls. Department of Mathematics and Statistics, University of New Mexico, Albuquerque (US), 4 May 1994. Unpublished.
- Michelsen, P.K., Vortices in η_i -modes. In: Transport in Fusion Plasmas, Aspenås, Göteborg (S), 13-16 June 1994. Unpublished.
- Michelsen, P.K., Two lectures 1) Fusion Energy and 2) Plasma Transport and drift wave instabilities. H.C. Ørsted Institute, Copenhagen (DK), 5 May 1994. Unpublished.

- Michelsen, P.K.; Karpman, V.I.; Lynov, J.P.; Juul Rasmussen, J., Modulational instability of plasma waves in two dimensions. Danish Physical Society spring meeting, Odense (DK), 2-3 Jun 1994. Unpublished. Abstract available.
- Nielsen, A.H.; Pécseli, H.L.; Rasmussen, J. Juul, Experimental investigations of turbulent transport in the edge plasma of the Q-machine. (Invited contribution). In: The 29 Nordic Plasma and Gas Discharge Symposium, Geilo (N), 31 January - 2 February 1994. Unpublished.
- Rasmussen, J. Juul, Vortical dynamics in plasmas and fluids. (Invited contribution). In: 21st EPS conference on controlled fusion and plasma physics. Abstracts of invited and contributed papers. 21. EPS conference on controlled fusion and plasma physics, Montpellier (FR), 27 Jun - 1 Jul 1994. Joffrin, E.; Platz, P.; Stott, P.E. (eds.), (The European Physical Society, Montpellier, 1994) p. 17
- Rasmussen, J. Juul, Vortical structures in plasmas and fluids. Institute seminar, Chalmers University of Technology, Institute for Electromagnetic Field Theory and Plasma Physics, Gothenburg (S), 11 January 1994. Unpublished.
- Rasmussen, J. Juul, Coherent structures in plasmas and fluids. (Invited contribution). In: 1994 International Conference on Plasma Physics, Foz do Iguacu, PR (Brazil), 31 October - 4 November 1994. Unpublished.
- Saffman, M.; Lading, L., A hybrid doppler/time-of-flight laser anemometer for turbulence measurements in a magnetized fusion plasma. Lecture at Max Planck Institut für Plasma Physik, Garching (D), 8 November 1994. Unpublished.
- Sutyriin, G.G.; Yushina, I.G.; Hesthaven, J.S.; Lynov, J.P.; Rasmussen, J.J., Non-linear interaction between a monopolar vortex and its Rossby wave wake. (Invited contribution). European Geophysical Society 19. general assembly, Grenoble (FR), 25-29 Apr 1994. Unpublished. Abstract available.

3 Work in Fusion Technology

3.1 Irradiation Effects

3.1.1 Accumulation of Irradiation-induced Defects in OFHC-copper Irradiated with 3 MeV Protons

(B.N. Singh, M. Eldrup and A. Horsewell and P. Ehrhart*, and F. Dworschak* (*Forschungszentrum Jülich, Germany))

In order to test the validity of the "Production Bias" model^{1,2)}, further irradiation experiments have been carried out. For this purpose, irradiations with 3 MeV protons were chosen since they are expected to produce not only single defects (interstitials and vacancies) but also multidisplacement cascades in copper. The defect clusters produced in these small cascades should, according to the production bias model, enhance the accumulation of vacancies in the form of voids (i.e. void swelling) compared to the void swelling observed in the case of 2.5 MeV electron irradiations where all vacancies and self-interstitials are produced as single defects. The accumulated void swelling (at a given dose level and irradiation temperature) in copper irradiated with 3 MeV protons should, on the other hand, be lower than that observed under fission neutron irradiations. This expectation is based on the fact that under neutron irradiations the clustering propensity is likely to be significantly higher (because of higher recoil energy) than that under 3 MeV proton irradiations.

To verify these predictions, 20 μm thick specimens of OFHC-copper were irradiated (at Jülich) with 3 MeV protons at 523 K to dose levels of about 0.002, 0.008 and 0.01 dpa. The displacement damage rate in these experiments was very similar to that under 2.5 MeV electron and fission neutron irradiations (i.e. 5×10^{-8} dpa (NRT) per second). The specimen thickness of 20 μm was chosen so that practically all incident protons should get out of the copper target. Post-irradiation defect microstructures were investigated using electrical resistivity, transmission electron microscopy (TEM) and positron annihilation spectroscopy (PAS).

The TEM investigations of the proton irradiated samples have not been completed yet. However, the preliminary results clearly demonstrate that the nucleation of voids under 3 MeV proton irradiation is substantially more efficient than under 2.5 MeV electron irradiation at ~ 523 K. In the case of proton irradiation, a void density of $\sim 9 \times 10^{19} \text{ m}^{-3}$ is reached at a dose level of ~ 0.002 dpa; the 2.5 MeV electron irradiation yielded a void density of about $2-12 \times 10^{18} \text{ m}^{-3}$ at a dose level of ~ 0.013 dpa. The void densities at 0.008 and 0.01 dpa were found to be $14 \times 10^{19} \text{ m}^{-3}$ and $9.5 \times 10^{19} \text{ m}^{-3}$, respectively. These densities are almost an order of magnitude lower than that observed in the case of neutron irradiation at similar doses at 523 K. The void sizes in the proton irradiated specimens were found to be similar to that in the case of neutron irradiations to similar doses. Thus, it is clear that the accumulation of vacancies under 3 MeV proton irradiations is more efficient than that under electron irradiation and is less efficient than that under neutron irradiations. This is a clear demonstration of the effect of the efficiency of intracascade interstitial clustering, as predicted by the production bias model.

The TEM examination of the proton irradiated specimens to a dose level of ~ 0.01 dpa also revealed that the void swelling was significantly enhanced in a relatively wide zone adjacent to grain boundaries. This is similar to the enhancement observed in the neutron irradiated specimens. It should be noted that no such enhancement was observed in the case of 2.5 MeV electron irradiations. These results are also consistent with the predictions of the production bias model.

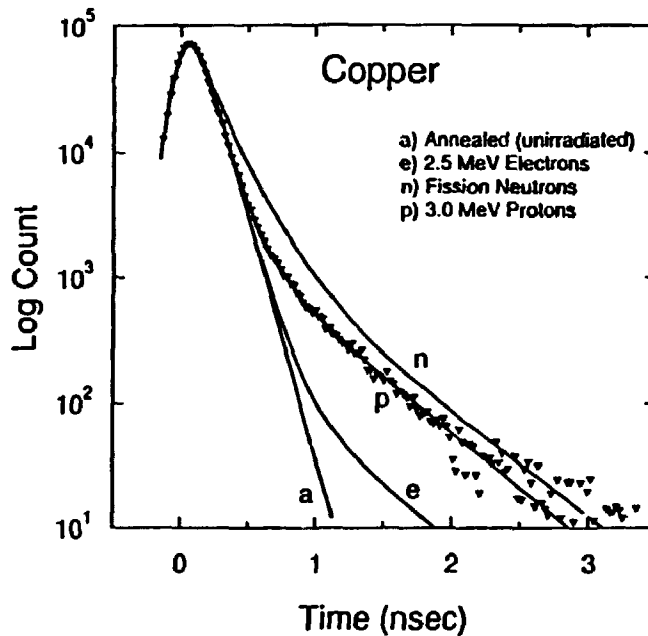


Figure 1. Positron lifetime spectra for copper: a) well annealed and unirradiated, e) electron irradiated, p) proton irradiated and n) neutron irradiated. All irradiation were done at ~ 523 K and to a dose level of ~ 0.01 dpa. For clarity, all spectra are shown by continuous curves obtained as fits to the experimental spectra. For the proton irradiated sample also the experimental points are shown.

The main results of the TEM investigations are confirmed by the positron annihilation measurements as illustrated in Fig. 1. The figure shows positron lifetime spectra for Cu irradiated with the three types of projectiles (all to about 0.01 dpa) as well as for annealed and unirradiated copper. All three spectra for irradiated specimens show a short-lived and one or two long-lived components. The latter arise from positrons which have been trapped in defects. The slopes of the long-lived parts of the spectra are roughly the same, reflecting positron lifetimes of about 500 picosec in all cases. This is characteristic lifetime of voids which are large enough to be seen by TEM. The intensity of this lifetime component for the proton irradiated sample is clearly intermediate between the electron and the neutron irradiated cases which gives evidence of a similar relationship between the void densities.

1) C.H. Woo and B.N. Singh, Phys. Stat. Sol. **B159** (1990) 609, Phil.Mag. **A65** (1992) 889.

2) B.N. Singh and A.J.E. Foreman, Phil. Mag. **A66** (1992) 975.

3.1.2 Effect of Neutron Irradiation on Microstructural Evolution and Mechanical Properties of TZM and Mo-5% Re Alloys

(B.N. Singh, J.H. Evans (University of London, U.K.), A. Horsewell, P. Toft, and D.J. Edwards (Pacific Northwest Laboratories, USA))

Because of the fact that molybdenum alloys are not included in the ITER R & D programme and therefore are not eligible for receiving ITER Credit, the ongoing European activities on these alloys were quietly frozen simply by allocating no new funding for the period beyond the end of 1993. However, we considered it to be prudent to round off the investigations that were already in progress.

The details of materials composition and experimental investigations together with preliminary results of tensile testing and microstructural investigations have been described in earlier reports and therefore will not be repeated here.

As reported last year, both TZM and Mo-5% Re alloys suffer almost a complete loss of ductility due to irradiation at 320 and 373 K to as low a dose level as ~ 0.16 dpa. Tensile testings at 523 K of specimens irradiated at 523 K demonstrated that these alloys had become so brittle that they broke already in the elastic regime. It was therefore decided to determine hardness of these alloys irradiated at 320, 373, 523, 623 and 723 K to a dose level of ~ 0.16 dpa; the results are plotted in Fig. 2. The TEM results on cluster density determined in specimens irradiated at various temperatures are also shown in Fig. 2. These results demonstrate two main features. Firstly, the hardness increases due to irradiation by about 30%, and secondly the increase in hardness is almost independent of irradiation temperature. Furthermore, a comparison of cluster density and hardness data (Fig. 2) shows that the clear large drop in cluster density with irradiation temperature is not reflected in the relative insensitivity of the hardness to irradiation temperature. This insensitivity is not consistent with the conventional mechanism of irradiation hardening based on the assumption that the irradiation-induced clusters may act as obstacles to dislocation motion (see later).

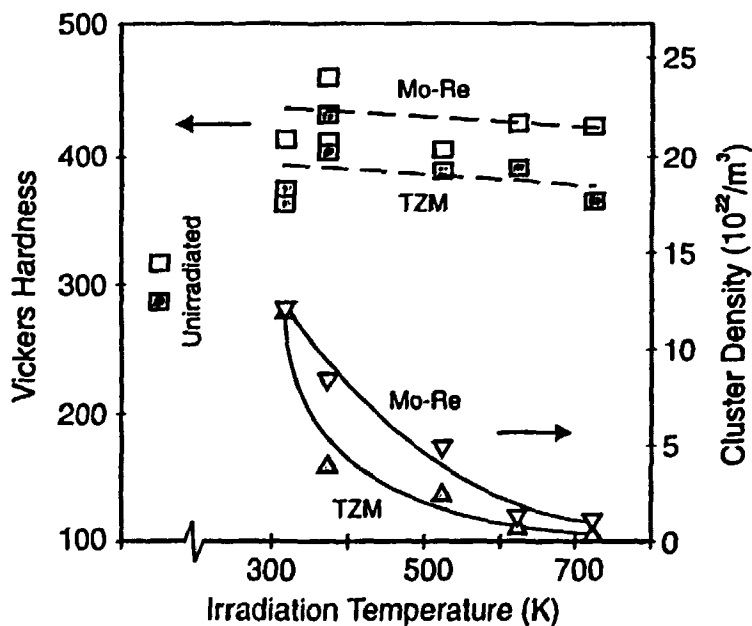


Figure 2. A comparison of Vickers hardness data with TEM loop densities for both TZM and Mo-5% Re as a function of irradiation temperature. Lines are drawn to guide the eye.

To gain further insight into the role of irradiation-induced defect clusters in the deformation behaviour, irradiated and tensile-deformed specimens were investigated by TEM. For the deformed Mo-5% Re specimens, no effects of the tensile test could be seen in the microstructure, i.e. there was no evidence of dislocation generation and motion, and the density and distribution of irradiation-induced clusters/loops were identical to the undeformed material. On the other hand, in the TZM specimens, there were strong indications of localized deformation within long and narrow bands which were free of any irradiation-induced microstructure (i.e. clear channels). It is important to note here that in the rest of the material there was no sign of dislocation generation and motion. Typical examples of the deformed microstructures in TZM and Mo-5% Re alloys are shown in Fig. 3. A clear implication of these observations is that the hardening due to irradiation is caused by the difficulties in generating dislocations and that the irradiation-induced clusters are not effective obstacles for dislocation motion.

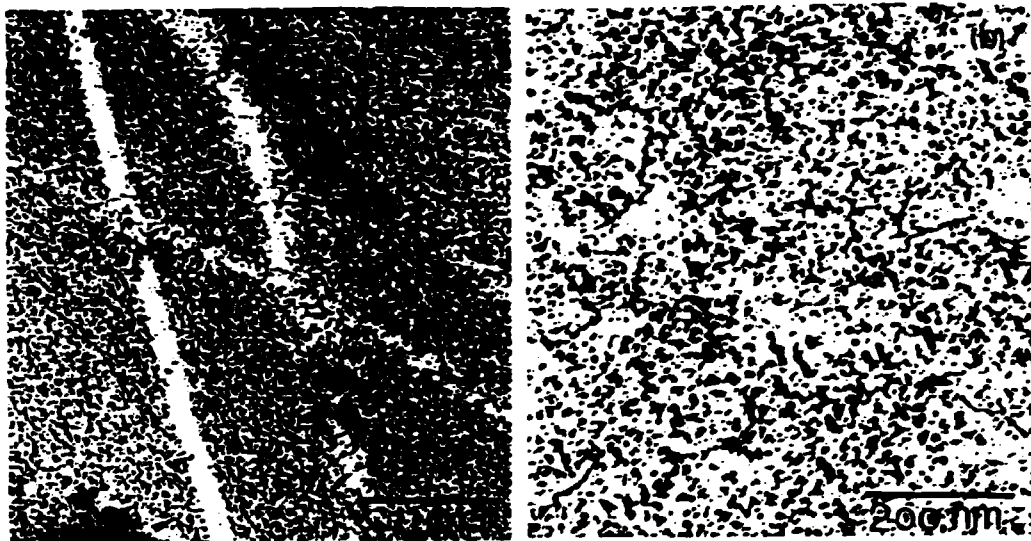


Figure 3. Micrographs taken after tensile testing of (a) TZM and (b) Mo-5% Re samples irradiated at 373 K. Clear channels where the irradiation-induced microstructure has been removed are visible in the TZM sample. Neither such clear channels nor deformation-induced dislocations were observed in the Mo-5% Re sample.

Voids were observed both in TZM and Mo-5% Re alloys at the irradiation temperatures of 623 and 723 K. It should be pointed out here that the void formation in these alloys at this low homologous temperature represents quite a different behaviour than in fcc metals and alloys where voids are observed at and above $0.3 T_m$ (e.g. Cu, Ni, austenitic stainless steels). In this context it should be also noted that on this same homologous temperature scale, the loop density in TZM and Mo-5% Re alloys induced by neutron irradiation is considerably lower than that in fcc metals (e.g. copper, nickel).

3.1.3 Temperature and Dose Dependencies of Microstructure and Hardness of Neutron Irradiated Copper

(B.N. Singh, A. Horsewell, P. Toft, and D.J. Edwards (Pacific Northwest Laboratories, USA))

The amount of experimental results on the evolution of defect microstructure and its impact on the deformation behaviour of polycrystalline copper is rather limited, particularly for elevated temperatures at which copper and its alloys may be employed in service (e.g. in fusion reactors). It is therefore of interest, not only from an academic but also from a practical point of view, to understand the correlation between irradiation-induced microstructure and mechanical properties of copper.

In the present investigations, tensile specimens of pure oxygen free high conductivity (OFHC) copper were irradiated with fission neutrons at temperatures in the range 320 to 723 K to fluences in the range 5×10^{21} to 1.5×10^{24} n/m² ($E > 1$ MeV) corresponding to displacement doses of 0.001 to 0.3 dpa (NRT). Prior to irradiation, all specimens were annealed in a vacuum of $< 10^{-5}$ torr at 823 K for 2 h. The resulting grain size was about 20 μ m and dislocation density was $\leq 10^{12}$ m⁻². Irradiated specimens were investigated by transmission electron microscopy (TEM) and quantitative determinations were made of defect clusters and cavities. The dose dependence of tensile properties of specimens irradiated at 320 K was determined at 295 K. Hardness measurements were made at 295 K on specimens irradiated at different temperatures and displacement doses. Microstructures of specimens were investigated in the as-irradiated as well as in the irradiated and deformed states.

Fluence (n/m ²) ($E > 1$ MeV)	Dose (dpa)	C_{cl} (dpa)	VHN (200 g)	σ_y (Mpa)	σ_{max} (Mpa)	ϵ_u (%)	ϵ_t (%)
0	0	-	40.1	59.0	210.5	8.3	9.0
5×10^{22}	0.1	5.3×10^{23}	79.4	193.5	250.0	5.1	6.5
5×10^{23}	0.1	6.7×10^{23}	99.5	292.5	-	-	3.3
1×10^{24}	0.2	6.6×10^{23}	105.0	310.0	-	-	2.1

Table 1. Cluster density (C_{cl}), Vickers hardness (VHN), yield stress (σ_y), maximum stress (σ_{max}), uniform elongation (ϵ_u) and total elongation (ϵ_t) for OFHC-copper before and after irradiation at 320 K to different dose levels.

The results of TEM investigations, hardness measurements and tensile tests on specimens irradiated at 320 K to different fluence (dose) levels are summarized in Table 1. The variation of tensile properties with the fluence is shown in Fig. 4 whereas the fluence dependence of Vickers hardness and cluster density are plotted in Fig. 5. It can be seen that the cluster density increases with increasing fluence but saturates already at a fluence level of 5×10^{23} n/m² ($E > 1$ MeV) (i.e. 0.1 dpa). However, both the yield strength and hardness keep on increasing until the fluence level of 1×10^{24} n/m² ($E > 1$ MeV) (i.e. 0.2 dpa) is reached. Another important feature to note is that the uniform elongation decreases rather rapidly with the neutron fluence and reaches a value of zero already at a dose level of 0.1 dpa (Fig. 4). This can be seen more clearly in Fig. 6 which shows that at the fluence level of 5×10^{23} n/m² ($E > 1$ MeV) (i.e. 0.1 dpa) the material loses its capacity to workharden; instead, the material begins to worksoften immediately after the yield point. This is a clear indication of the fact that the plastic deformation occurs

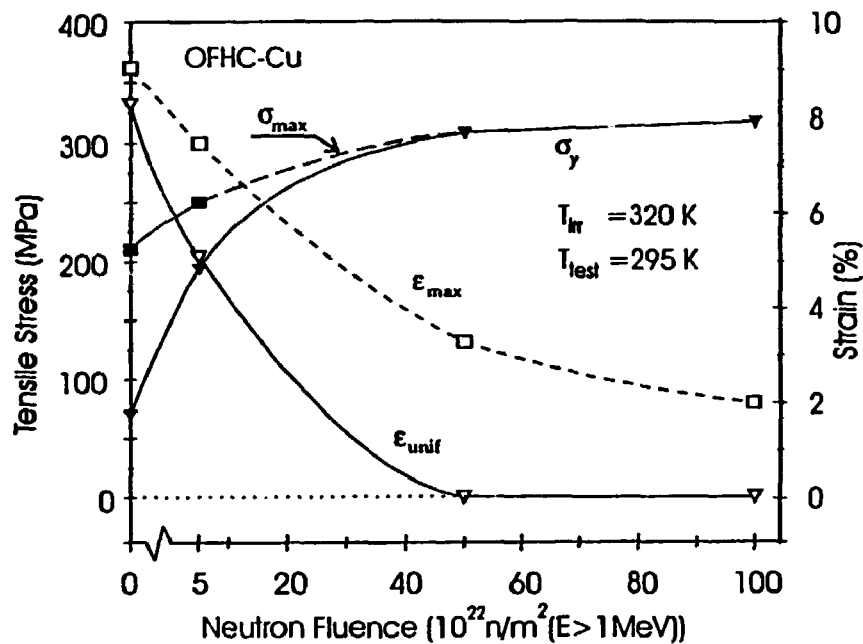


Figure 4. Fluence dependence of tensile properties of OFHC-copper irradiated at 320 K and tested at 295 K. Note a sharp increase in the yield stress, σ_y , and a drastic decrease in the uniform elongation with increasing fluence level.

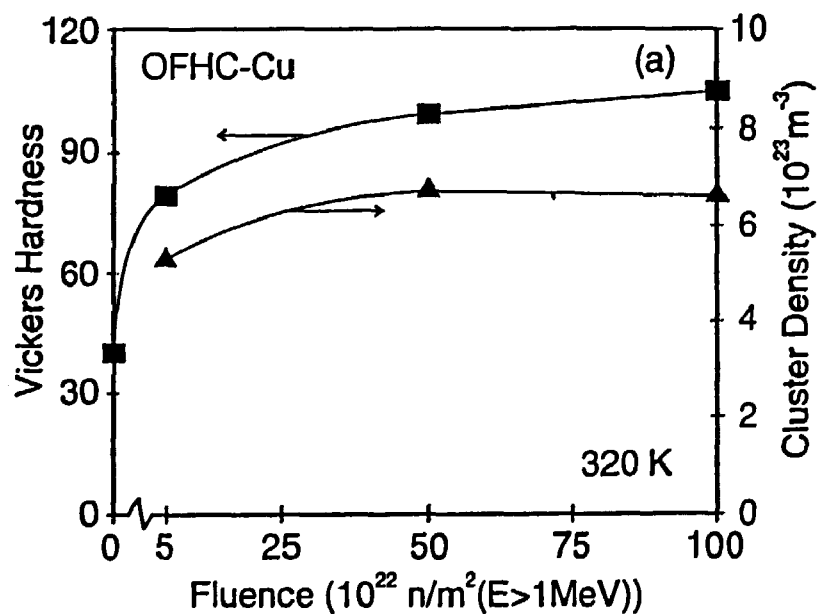


Figure 5. Variation of room temperature hardness and cluster density with neutron fluence in OFHC-copper irradiated at 320 K.

in a localized fashion.

Figure 7 shows the temperature dependence of Vickers hardness and cluster density at a dose level of $\sim 0.3 \text{ dpa}$. It is evident that the decrease in hardness with increasing temperature is considerably smaller than the decrease in cluster density.

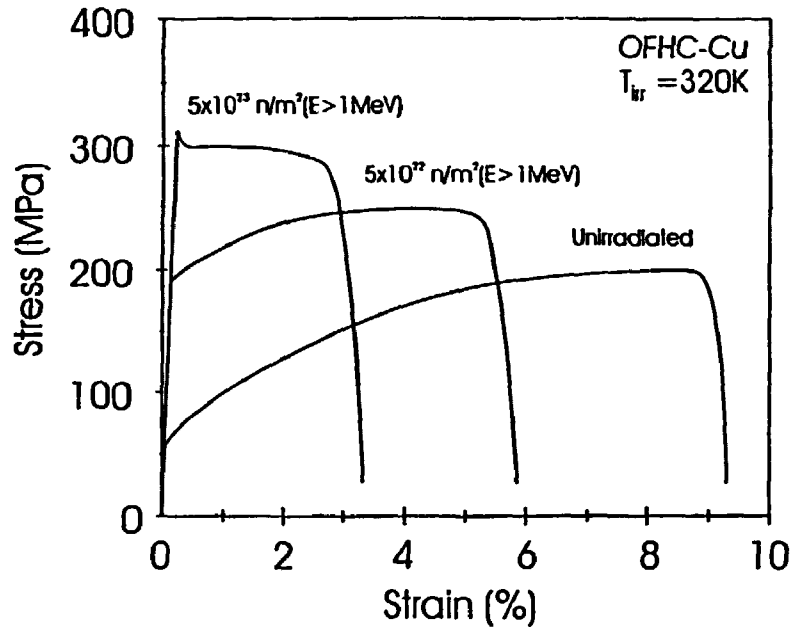


Figure 6. Stress-strain curves for OFHC-copper irradiated to different fluence levels at 320 K and tested at 295 K. For comparison, the stress-strain curve for the unirradiated reference specimen is also shown. Note the lack of work hardening and uniform elongation in the specimen irradiated to a fluence level of $5 \times 10^{23} \text{ n/m}^2$ ($E > 1 \text{ MeV}$); a similar behaviour is observed at higher fluences.

The decrease in the hardness value is largest between the irradiation temperatures of 320 and 523 K. The decrease in the cluster density in the same temperature range, on the other hand, is very small. In contrast, the cluster density decreases rather rapidly at temperatures between 523 and 623 K, whereas the decrease in the hardness value in the same temperature range is very small. In other words, there is a lack of direct correlation between the hardness and the cluster density.

In order to understand the observed deformation behaviour, post-deformation investigations were carried out on irradiated as well as unirradiated specimens. Scanning electron microscopy of fracture surfaces showed indications of plastic deformation in the grains in the unirradiated specimens and the specimen irradiated to 0.01 dpa. The specimens irradiated to 0.1 and 0.2 dpa, on the other hand, showed clear evidence of transgranular cleavage in the fracture surfaces. Thus, the loss of ductility at higher doses appears to be caused by grain boundary sliding and separation and not the grain boundary embrittlement due to impurity segregation. The TEM investigations of deformed specimens showed the evidence of dislocation generation and interactions during deformation of the unirradiated specimens and specimens irradiated to low doses. In specimens irradiated to higher doses, on the other hand, no indication of dislocation generation was observed.

The analysis of mechanical properties and microstructural evidence suggests that the increase in the initial yield stress due to irradiation is unlikely to be caused by the Orowan type of hardening mechanism. Instead, we propose that the increase in the initial yield stress due to irradiation may arise from the strong pinning of dislocation sources (e.g. grown-in dislocations).

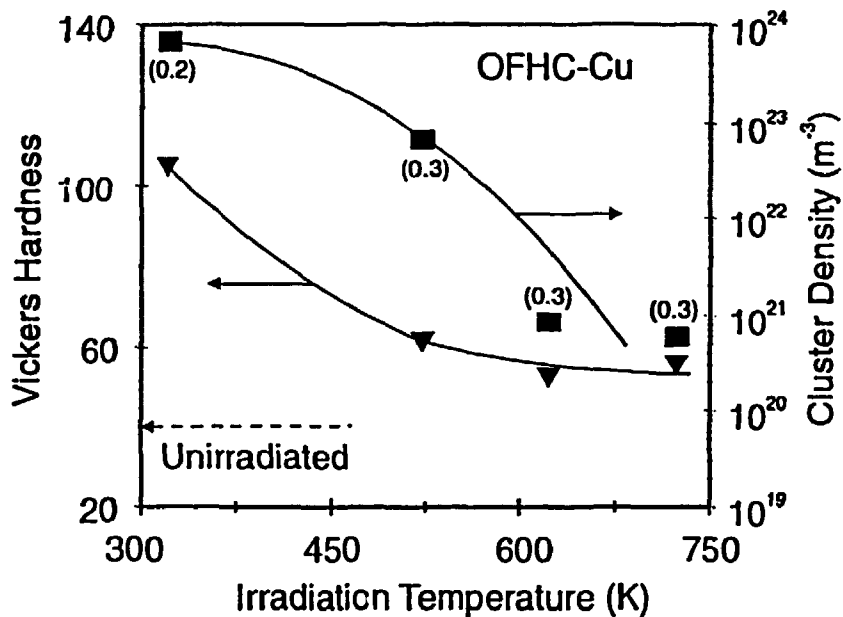


Figure 7. Temperature dependence of room temperature hardness and cluster density in OFHC-copper neutron irradiated to 0.2 and 0.3 dpa; note that although there is a large decrease in the cluster density between 523 and 723 K, there is no significant change in the hardness values. The number in brackets refer to displacement damage in dpa (NRT).

3.1.4 Effects of Neutron Irradiation on Microstructure and Tensile Properties of Copper Alloys

(B.N. Singh, P. Toft, and D.J. Edwards (Pacific Northwest Laboratories, USA))

At present, copper alloys (Cu-Al₂O₃, CuCrZr and CuNiBe) are being considered as candidate materials for the first wall and divertor components of ITER (International Thermonuclear Experimental Reactor). The present investigations of the effects of neutron irradiation on microstructures and mechanical properties of these alloys is a part of ITER research and development programme.

Tensile specimens of the candidate alloys Cu-Al₂O₃, CuCrZr and CuNiBe were irradiated with fission neutrons in the DR-3 reactor at Risø with a flux of 2.5×10^{17} n/m²s ($E > 1$ MeV) (i.e. dose rate of $\sim 5 \times 10^{-8}$ dpa/s) to fluences of 5×10^{22} , 5×10^{23} and 1×10^{24} n/m² ($E > 1$ MeV) (i.e. displacement doses of 0.01, 0.1 and 0.2 dpa) at 320 K. Prior to irradiation, the tensile specimens of CuNiBe and CuCrZr were solution annealed at 1223 K for 1 hour in a vacuum of $K \leq 10^{-5}$ torr and then water quenched. These solution annealed (SA) specimens were aged at 748 K for 30 min in a vacuum of $< 10^{-5}$ torr and water quenched. The Cu-Al₂O₃ (CuAl25) specimens, on the other hand, were irradiated in the as-cold worked state. Tensile properties and Vickers hardness of both irradiated and unirradiated specimens were determined at 295 K. Pre- and post-deformation microstructures of irradiated as well as unirradiated specimens were examined using a transmission electron microscope (TEM). The fractured surfaces of tensile tested specimens were investigated in a scanning electron microscope (SEM).

The deformation behaviour of the three alloys in unirradiated as well as irradiated states is illustrated in Fig. 8. Figs. 8(a) and 8(b) show the stress-strain curves for CuNiBe and CuCrZr and CuNiBe and Cu-Al₂O₃ (CuAl25) alloys, re-

spectively. It is clearly seen (Fig. 8(a)) that even negatively low dose irradiations cause significant increases in the yield strength of both CuCrZr and CuNiBe alloys. However, in the case of both alloys, the ductility decreases very markedly with increasing irradiation dose and already at the dose level of 0.2 dpa, the uniform elongation becomes zero (Fig. 8(a)). In other words, these materials lose their capacity to deform plastically in a homogeneous fashion. It is interesting to note that the CuNiBe alloy is considerably stronger than the CuCrZr alloy, both in the unirradiated and irradiated conditions. This is consistent with the TEM results showing that the density of precipitates in CuNiBe is considerably higher than that in CuCrZr alloy.

Fig. 8(b) shows the stress-strain curves for CuNiBe and Cu-Al₂O₃ (CuAl25) alloys tested in irradiated and unirradiated conditions. The results clearly demonstrate that the CuNiBe alloy is stronger than the Cu-Al₂O₃ alloy both in irradiated as well as unirradiated conditions. It is interesting to note here that the low-dose irradiation of the cold-worked Cu-Al₂O₃ (CuAl25) alloy causes a decrease in the yield stress and an increase in the uniform elongation (Fig. 8(b)). The yield stress then increases and the uniform elongation decreases again at higher doses. The initial decrease in the yield stress may be due to irradiation-induced partial recovery or relaxation of the cold-worked dislocation microstructure. In Fig. 8(b) the stress-strain curve for the as-extruded Cu-Al₂O₃ (CuAl25) alloy tested in the unirradiated condition is also shown. The TEM examination of this material shows that the dislocation microstructure in the as-extruded specimens is in fully relaxed and recovered state.

The results of Vickers hardness measurements on all three alloys in both irradiated and unirradiated conditions showed the same general trend as demonstrated by the tensile tests. In other words, the CuNiBe alloy was found to be harder than both Cu-Al₂O₃ and CuCrZr alloys and the Cu-Al₂O₃ was found to be harder than CuCrZr alloy.

Detailed TEM investigations were carried out on specimens of Cu-Al₂O₃, CuNiBe and CuCrZr alloys in irradiated and unirradiated conditions. Fig. 9 shows, for example, the variation of irradiation induced cluster density in Cu-Al₂O₃ with the neutron fluence. As in the case of pure copper, the cluster density increases with the fluence and appears to be reaching a saturation value at a fluence level of 1×10^{24} n/m² ($E > 1$ MeV). The size distributions of stacking fault tetrahedra (SFTs) were determined for each irradiation dose. The results showed that the size distribution is not influenced in any significant way by the irradiation dose; an example of such a size distribution determined for Cu-Al₂O₃ alloy irradiated to a dose level of 0.2 dpa (1×10^{24} n/m² ($E > 1$ MeV)) is shown in Fig. 10.

The TEM examinations of the irradiated and deformed specimens of all three alloys showed that at higher doses the lack of uniform elongation (i.e. homogeneous plastic deformation) appears to be related to the fact that at these doses there is difficulty in dislocation generation during deformation. This may arise due to a strong pinning of grown-in dislocations (dislocation sources) by defect clusters at or around them. The SEM examinations of the fractured surfaces of the irradiated and tensile tested specimens demonstrated that the loss of ductility may be related to the intrinsic weakness of the grain boundaries and hardness of the grain interiors and not to the grain boundary embrittlement due, for example, to impurity segregation.

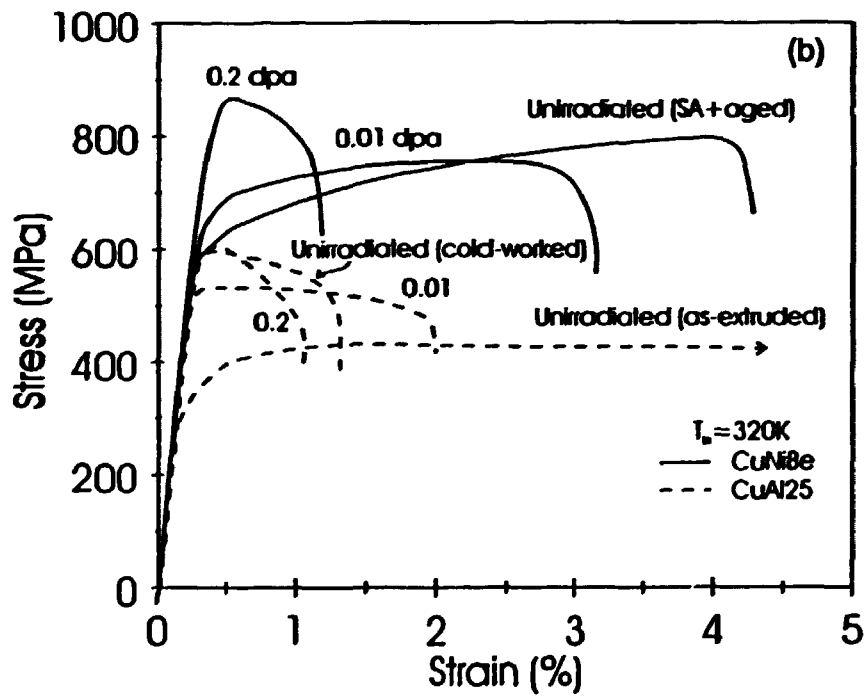
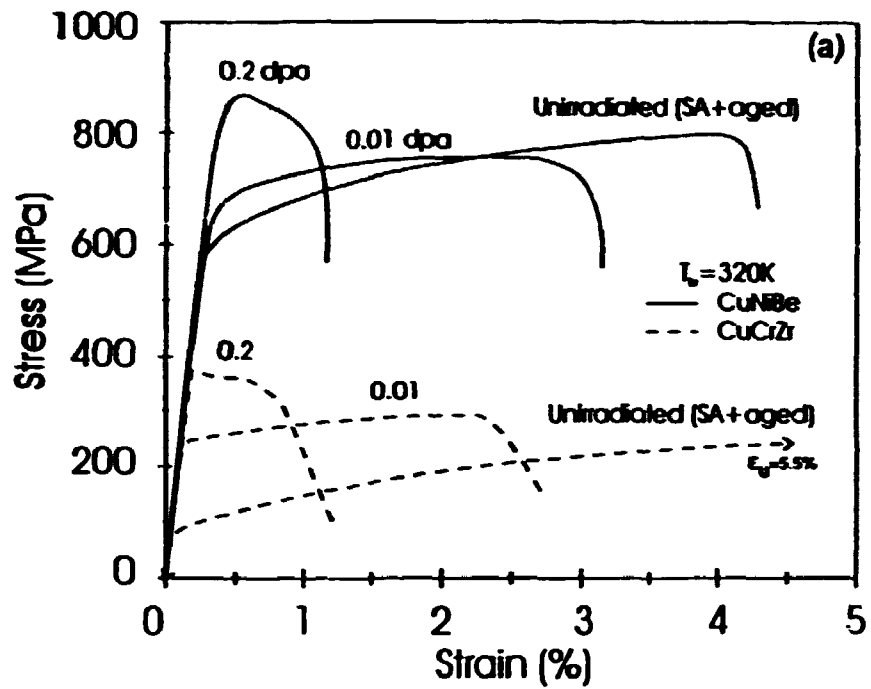


Figure 8. Stress-strain curves for copper alloys neutron irradiated at 320 K to displacement dose levels of 0.01 and 0.2 dpa. For comparison, the stress-strain curves for unirradiated specimens are also shown. All specimens were tested at 295 K: (a) CuNiBe and CuCrZr alloys and (b) CuNiBe and Cu-Al₂O₃ (CuAl25) alloys.

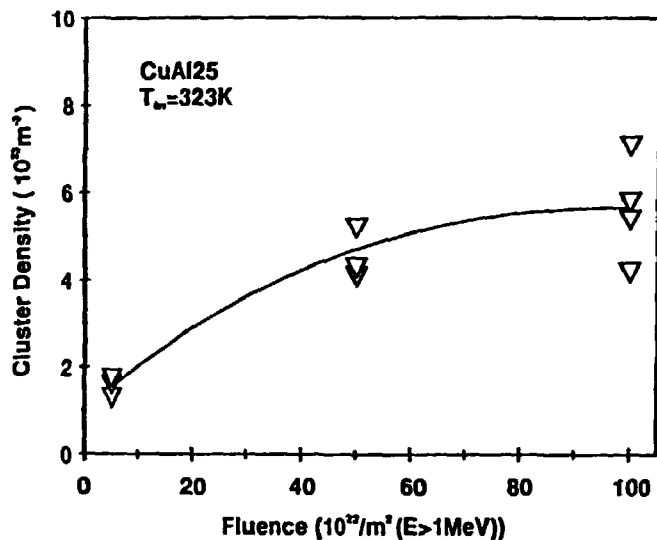


Figure 9. Fluence dependence of defect cluster density for the Cu-Al₂O₃ (CuAl25) alloy irradiated at 323 K.

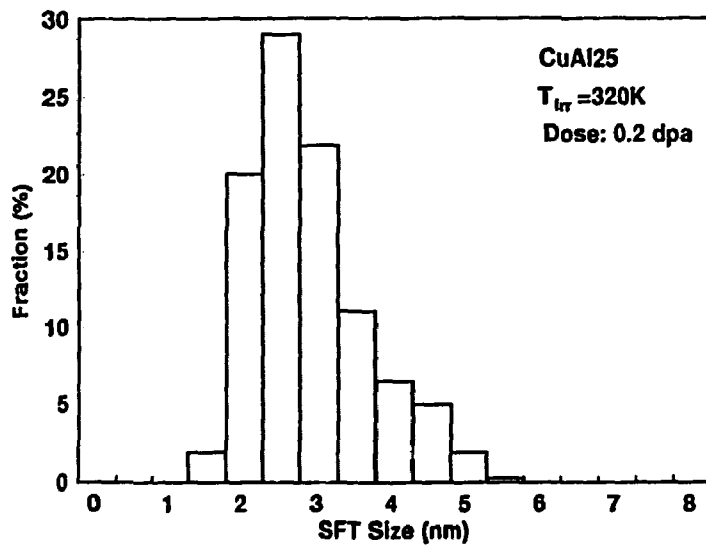


Figure 10. Size distribution of stacking fault tetrahedra (SFT) in the Cu-Al₂O₃ (CuAl25) alloy irradiated at 320 K to a dose level of 0.2 dpa.

3.1.5 Low Cycle Fatigue Behaviour of a Cu-Cr-Zr Alloy at Room Temperature

(J.F. Stubbins*, K. Leedy*, and B.N. Singh (*University of Illinois, USA))

Room temperature fatigue tests were performed on CuCrZr subsize and ASTM standard size specimens to determine the fatigue response and lifetime. The fatigue tests were run in strain control mode. The stress amplitude as a function of cycle number and the total number of cycle to failure were determined.

The CuCrZr specimens were examined by optical and transmission electron-microscopy to establish the base microstructure. This examination revealed a number of large Cr-based precipitates (EDX showed Cr only). These were in addition to a finer scale CrZr precipitate structure which was non-uniformly distributed in the specimens which were examined. The initial dislocation densities were low.

The fatigue behaviour is compared to OFHC-Cu and Cu-Al₂O₃ (CuAl25) in Fig. 11. It should be noted that the initial strength of the CuCrZr alloy was not much higher than OFHC-Cu and the fatigue performance (strain vs. cycles to failure curve) shows that the fatigue performance of the alloy is between OFHC Cu (worse) and CuAl25 (better). In most fatigue studies, weaker, more ductile alloys outperform their higher strength, less ductile counterparts in the low cycle fatigue regime (100-10,000 cycles to failure) and under-perform the stronger material in the high cycle range. However, in the present studies, the stronger material (CuAl25) out-performs the more ductile Cu alloys over the entire range of behaviour.

For the greatest part, the CuCrZr material, which was rather soft, exhibited initial cyclic strain hardening followed by an extended plateau in the stress response. The stress fell only near the failure point. However, in two specimens, the initial cyclic strain hardening behaviour was followed by a slow softening until a more rapid decrease in stress near failure. The reason for this behaviour is not certain, but is under further investigation.

The results shown in Figs. 11(a) and 11(b) do indicate that specimen size exerts influence on the failure lives of all three materials. In all cases, the failure lines are shorter for the smaller size specimens when compared to that of larger (standard size) specimens tested under nominally identical experimental conditions. The reasons for the difference in fatigue lives as a function of specimen size are not readily apparent, but may be due in parts to differences in surface to volume ratios. Since the fatigue process is dominated by surface effects and since fatigue cracks initiate and grow from the surface, a larger relative surface to volume ratio (i.e. smaller specimen diameter) could lead to a faster accumulation of fatigue damage even when the effect of gauge length is taken into account. Thus, although useful fatigue data can be obtained from reduced size specimens, complementary results on standard size specimens are needed for comparison.

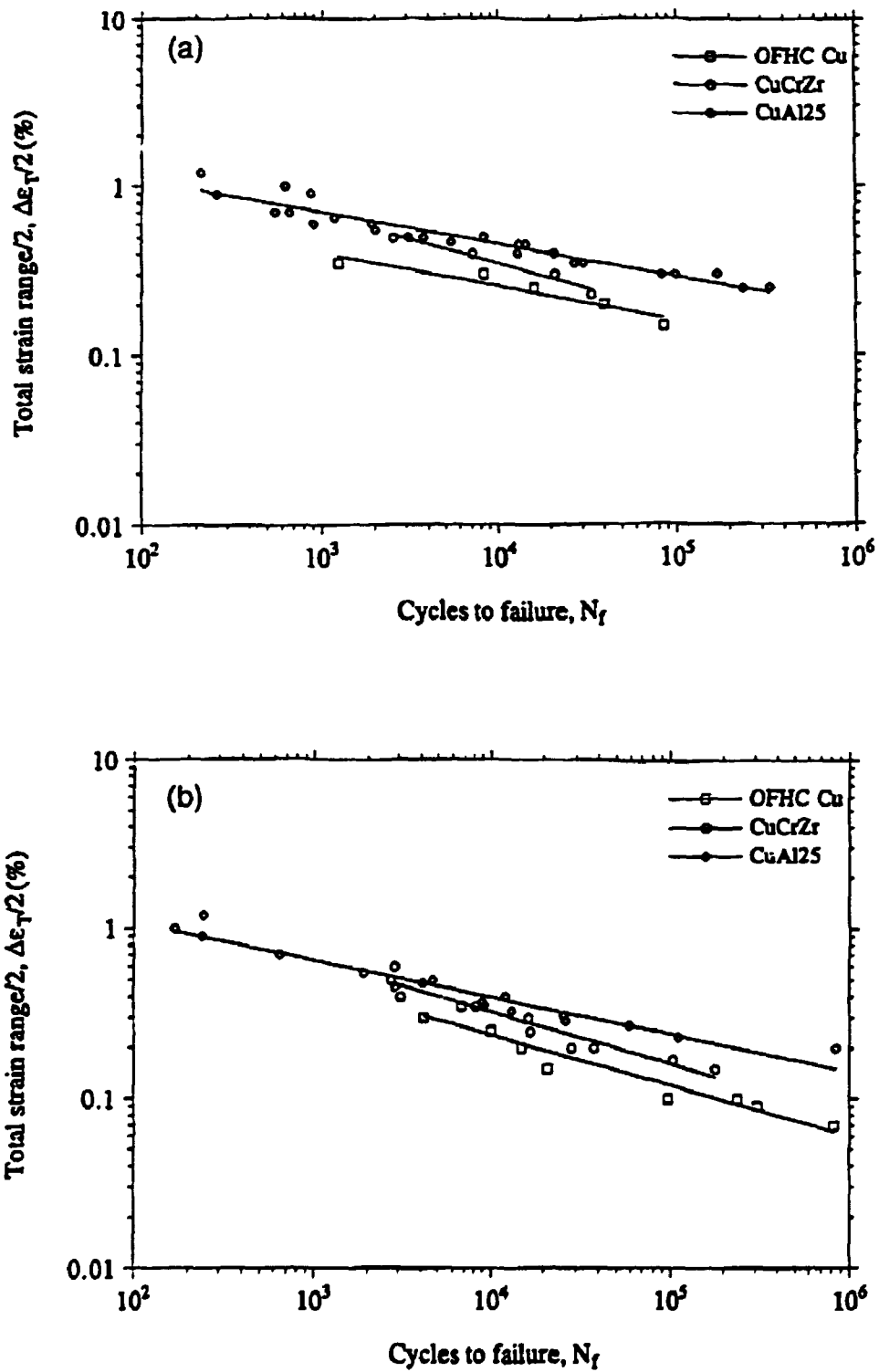


Figure 11. Low cycle fatigue behaviour of unirradiated OFHC-Cu, CuCrZr and Cu-Al₂O₃ (CuAl₂₅) specimens of two different sizes; all tests were carried out at 298 K in air: (a) standard size specimens and (b) subsize specimens.

3.1.6 Cascade-induced Source Hardening

(B.N. Singh and A.J.E. Foreman (Harwell Laboratory, England))

Deformation experiments on irradiated copper and copper alloy (e.g. see Figs. 6

and 8) have shown that even a relatively low dose irradiation with fission neutrons at temperatures below the annealing stage V causes drastic changes in mechanical properties. The initial yield stress is greatly increased and the ductility is reduced to practically zero value due to irradiation. Instead of workhardening, the irradiated materials exhibit worksoftening which is associated with very inhomogeneous and localized deformation. It should be pointed out that this kind of behaviour is observed even in complicated materials such as ferritic and austenitic stainless steels.

TEM investigations of irradiated materials prior to deformation commonly show that the pre-existing dislocations become heavily decorated with small dislocation loops during the neutron irradiation. Furthermore, the post-deformation microstructural investigations of irradiated materials to the dose level where deformation occurs in inhomogeneous and localized fashion show a complete lack of homogeneous dislocation generation during deformation even at very high stresses. It is important to note, however, that under these conditions the localized deformation causes the formation of cleared channels. Within these channels, dislocations move very readily and rapidly and the irradiation-induced defect clusters do not appear to act as obstacles to dislocation motion.

Thus, experimental observations do not appear to be consistent with the traditional hardening model based on Orowan type of hardening mechanism where defect clusters are assumed to be obstacles to dislocation motion. Experimental results provide evidence for the fact, on the other hand, that in the irradiated materials the pre-existing dislocations are unable to act as dislocation sources. Once generated, they move without much hindrance through the defect clusters as shown by the cleared channels.

In order to understand the observed hardening behaviour, various stages in the interaction of defect clusters/loops with a straight (stationary or mobile) dislocation segment have been identified. Calculations have been initiated to determine the strength of the dislocation-loop attractive interaction, stand-off distances at which small loops may change their Burgers vector to facilitate the coalescence with the dislocation segment, and the break-away stress necessary to unlock the dislocations decorated with small clusters/loops. Preliminary results show that in pure fcc metals an undissociated dislocation segment may provide quite extensive attractive sweeping of the glissile clusters. The estimate of the stress needed to change the Burgers vector of small loops indicates that the lower bound to the stand-off distance is likely to be when the loop is quite close to the dislocation segment. Thermal activation would be expected to assist the process when the loops are very small, so that a larger stand-off distance might be expected at higher temperatures. The effect of temperature on the magnitude of the stand-off distance is under investigation.

In the present work the proposed model considers that the increase in the initial yield stress due to irradiation may rise due to high stresses necessary for unlocking the decorated dislocations. An estimate has been made of the stress required to pull a straight dislocation segment from a row of small defect cluster loops that are uniformly spaced along its length (based on the small loop approximation). The break-away stress is found to depend on the loop size as well as on the magnitude of the stand-off distances. The estimates indicate that the observed yield stress increase of 240 Mpa in irradiated copper could be explained if the straight dislocations were to be decorated by ~ 2.5 nm diameter loops at a stand-off distance ~ 5 nm and with an average spacing along the length of the dislocation ~ 5 nm. This appears to be entirely reasonable and is not dissimilar to the dislocation decoration observed in copper.

3.1.7 Stochastic Annealing Simulation of Free Defect Production in Irradiated Metals

(H.L. Heinisch (Pacific Northwest Laboratory, USA) and B.N. Singh)

Under cascade-producing irradiation by high energy neutrons or charged particles, only about 20 - 30% of the initially produced defects formed by displaced atoms survive the thermal spike phase as stable isolated or clustered defects. After subsequent intracascade annealing at the crystal temperature, a fraction of the surviving defects escape to contribute to the population of free defects that are available to migrate throughout the metal and cause microstructural changes. Atomic-scale computer simulations of free defect production are being done using several simulation techniques in tandem to cover the wide ranges of time and distance scales involved. Molecular dynamics simulations are used to generate the initial damage in displacement cascades, while stochastic annealing simulations are used to model the subsequent migration of the defects on more macroscopic time and size scales. Using this approach, we have shown that the temperature dependence of free defect production in noninteracting, isolated cascades in copper shows a differential in the fractions of free vacancies and interstitial defects escaping from the cascade above recovery Stage V, i.e. at about three tenths of the melting temperature (Fig. 12). This differential, a consequence of the direct formation of interstitial clusters in cascades and the relative thermal stability of vacancy and interstitial clusters during subsequent annealing, is the basis for the production bias mechanism of void swelling in irradiated metals. The escape of 80% present simulations is in good agreement with results of an analytical calculation using a spherically symmetric model of a cascade¹⁾.

1) B.N. Singh and A.J.E. Foreman (1992). *Phil. Mag.* **A66**, 975.

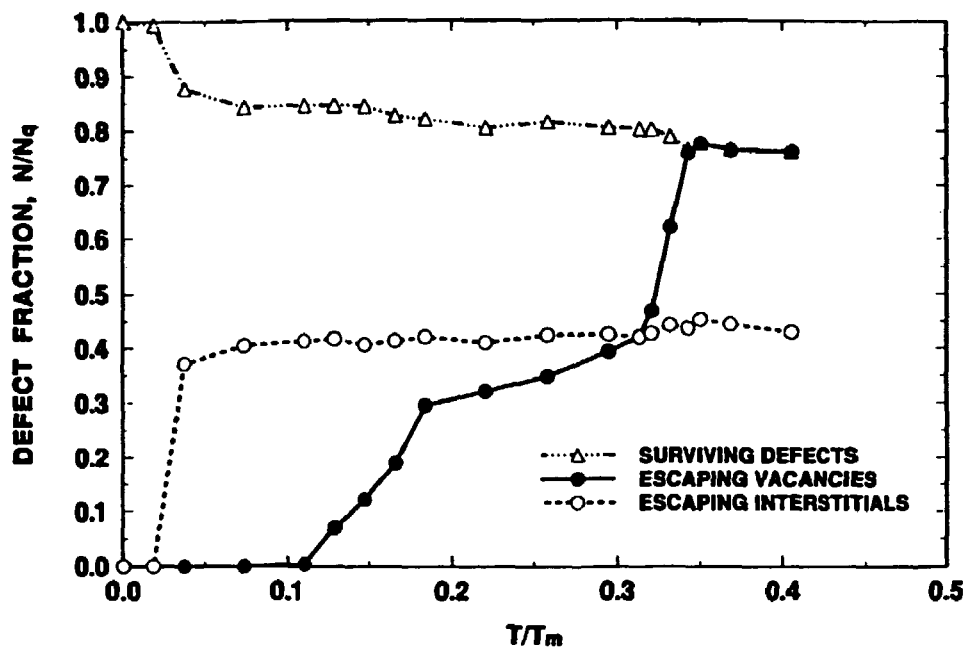


Figure 12. Annealing of isolated 25 KeV cascades in copper. The defect fractions for the total number of defects surviving recombination and the vacancies and self-interstitial atoms that escape from the cascades are plotted as a function of annealing temperature. The defect fractions are relative to the number of point defects surviving the thermal spike at the end of the molecular dynamics simulation. The temperatures are relative to the experimental melting temperature of copper.

3.1.8 Helium Implanted Copper: Correlation Between TEM and Positron Annihilation Data

(M. Eldrup, B.N. Singh and A. Möslang (Kernforschungszentrum, Karlsruhe, Germany))

As a supplementary technique to transmission electron microscopy (TEM) the positron annihilation spectroscopy (PAS) has the advantage of being able to detect submicroscopic vacancy type defects as well as defect clusters which can be observed by TEM. It is also possible to get information on gas densities in bubbles in metals, in the present case He in cavities in copper. We have previously reported PAS results on He implanted copper which showed the transition from submicroscopic vacancy clusters to He bubbles that could also be observed by TEM.

In order to extract quantitative information on e.g. bubble or void densities, it is necessary to establish a correlation between a measurable quantity, e.g. the trapping rate of positrons (κ) into the cavities and the cavity density (C_v). To a good approximation $\kappa = \mu C_v$, where μ is the specific rate of trapping of positrons into the cavities. The specific trapping rate in copper has been estimated for different cavity sizes by correlating positron lifetime and TEM measurements primarily on copper specimens in which bubbles were created by He implantation, but also on copper in which voids were created by electron, neutron or proton irradiation. Figure 13 shows the specific trapping rate as a function of cavity size for three-dimensional vacancy clusters as derived from these measurements. A previous estimate of the cavity size dependence of the specific trapping rate for Cu, based on similar results for Al, is plotted together with an estimated uncertainty

band. Although there is appreciable scatter of the points, the general behaviour is rather well-defined. For large cavities the trapping rate is expected to be diffusion controlled, and in fact, the present results compare favourably with independent positron diffusion measurements. Based on the data for Al and Cu it is now possible to make reasonable estimates of the specific trapping rates for a number of other metals as well, without having to first make the rather tedious correlation between PAS and TEM data as done here.

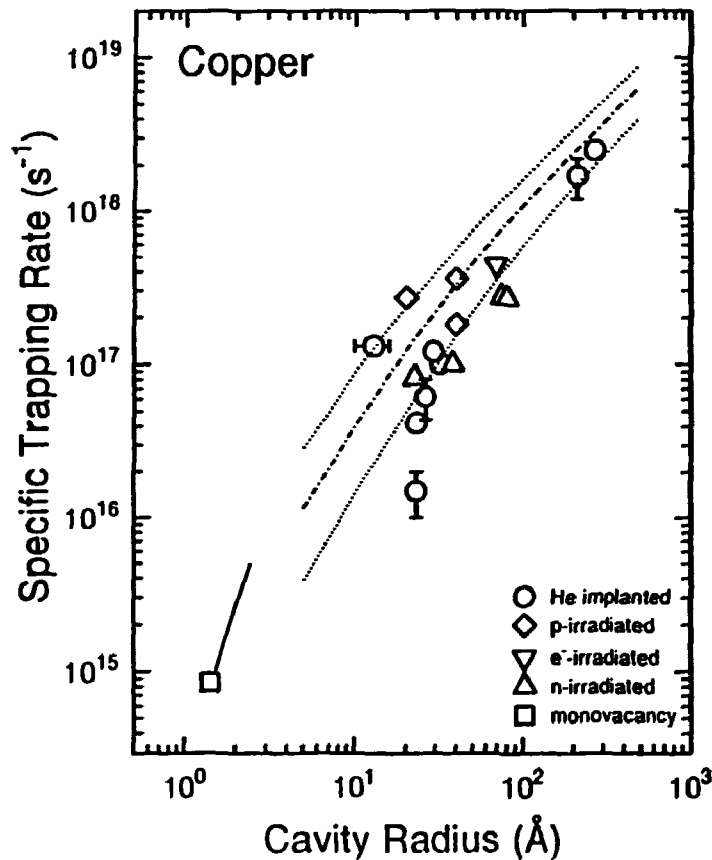


Figure 13. The specific trapping rate for positron trapping into cavities as a function of cavity radius, deduced by a combination of PAS and TEM data. The cavities were created by irradiation with He, neutrons, protons or electrons as indicated in the figure. The curves represent previous estimates of the rate and the associated error band.

The He density in the bubbles can be estimated from the positron lifetime, using the relationship: $\tau = 500-24 n_{\text{He}}$ where τ is the positron lifetime in ps and n_{He} the He density in 10^{28} m^{-3} . The He density can also be estimated from TEM data in two different ways. One is to assume all the He in the specimen to be present in the bubbles the total volume of which equals the swelling. The other is to assume the bubbles to be in thermal equilibrium, then from the bubble size to calculate the equilibrium pressure and from this obtain the He density via the equation of state. A comparison for as-implanted Cu specimens of PAS densities with those obtained by the first TEM method show a very large scatter of points. However, using the assumption of thermal equilibrium bubbles for the TEM estimate, a fairly good agreement is obtained. This is shown in Fig. 14. These results indicate that in several of the specimens He is not only trapped in visible bubbles, but also in other defect.

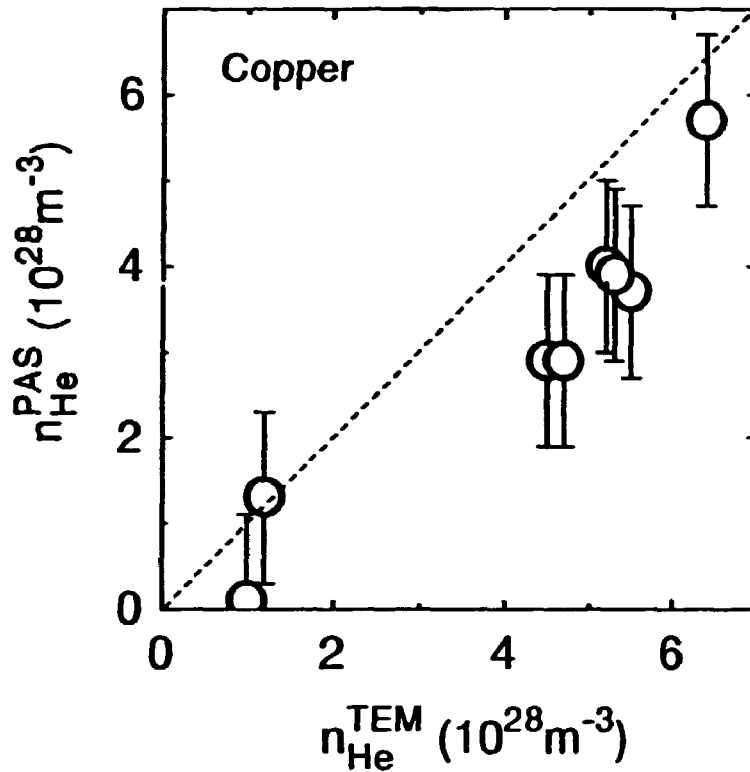


Figure 14. The correlation between the He density in bubbles in Cu as derived from PAS (n_{He}^{PAS}) and from TEM assuming equilibrium bubbles (n_{He}^{TEM}).

3.2 Water Radiolysis under ITER Conditions

3.2.1 ITER CTA Task T50: Primary Water Loop Technology

This task is the continuation of the task NWC1-1 aiming at calibrating the computer code CHEMSIMUL to allow reliable extrapolation to ITER conditions. The computer simulation refers to irradiation experiments performed by CEA in the frame of the present T50 and described in CEA's proposal dated March 1994. The task includes

- Simulation of radiolysis of borated water capsules at 120°C.
- Influence of dose rate on the radiolytic yields $G(O_2)$ and $G(H_2O_2)$.
- Literature review on methods for suppression of water decomposition in reactors.

3.3 Participants in the Fusion Technology Work

Scientific Staff

Bjergbakke, E. (part time, < 10%)
Eldrup, Morten (part time, ~ 60%)
Horsewell, Andy (part time, ~ 20%)
Johansen, B.S. (part time, ~ 10%)
Singh, Bachu N.
Toft, Palle (part time, ~ 30%)

Technical Staff

Lindbo, Jørgen (part time, ~ 10%)
Nilsson, Helmer (part time, ~ 10%)
Olsen, Benny
Pedersen, N.J. (part time, ~ 30%)

Guest Scientists

Edwards, D.J., Pacific Northwest Laboratories, Richland, U.S.A.
Evans, J.H., University of London, England
Woo, C.H., Atomic Energy of Canada Ltd., Pinawa, Canada
Foreman, A.J.E., Harwell Laboratory, Harwell, England

Short Time Visitors

Zinkle, S.J., Oak Ridge National Laboratory, Oak Ridge, U.S.A.
Golubov, S.I., Institute of Physics and Power Engineering, Obninsk, Russia

3.4 Publications and Conference Contributions

3.4.1 Publications

- Garner, F.A., Singh, B.N. (1994). Influence of nickel and beryllium content on swelling of copper irradiated in COBRA-1A. In: Fusion materials. Semiannual progress report for the period ending March 31, 1994. DOE-ER-0313-16, p. 364-367.
- Heinisch, H.L., Singh, B.N., Diaz de la Rubia, T. (1994). Calibrating a multi-model approach to defect production in high energy collision cascades. *J. Nucl. Mater.* v. 212/215 p. 127-131.
- Singh, B.N., Eldrup, M., Mslang, A. (1994). Effect of hot helium implantation in copper on bubble formation within grains and on grain boundaries. In: Effects of radiation on materials. ASTM 16. International Symposium, Aurora, CO (US), 1992. Kumar, A.S., Gelles, D.S., Nanstad, R.K., Little, E.A. (eds.), (ASTM, Philadelphia, PA, 1993) (ASTM Special Technical Publication, 1175) p. 1061-1073.
- Singh, B.N., Foreman, A.J.E., Trinkaus, H. (1994). Production bias driven defect accumulation in the transient regime. *Plasma Devices and Oper.* v. 3 p. 115-129.
- Singh, B.N., Horsewell, A. (1994). Effects of fission neutron and 600 MeV proton irradiations on microstructural evolution in OFHC-copper. *J. Nucl. Mater.* v. 212/215 p. 410-415.
- Singh, B.N., Horsewell, A., Toft, P., Evans, J.H. (1994). Effect of neutron irradiation on microstructure and tensile properties of TZM and Mo-5% Re alloys. *J. Nucl. Mater.* v. 212/215 p. 1292-1297.
- Singh, B.N., Trinkaus, H., Woo, C.H. (1994). Production bias and cluster annihilation: Why necessary? *J. Nucl. Mater.* v. 212/215 p. 168-174.
- Singh, B.N., Zinkle, S.J. (1994). Influence of irradiation parameters on damage accumulation in metals and alloys. *J. Nucl. Mater.* v. 217 p. 161-171.
- Singhal, A., Stubbins, J.F., Singh, B.N., Garner, F.A. (1994). Room temperature fatigue behaviour of OFHC copper and CuAl25 specimens of two sizes. *J. Nucl. Mater.* v. 212/215 p. 1307-1312.
- Trinkaus, H., Naundorf, F., Singh, B.N., Woo, C.H. (1994). On the experimental determination of the migrating defect fraction under cascade damage conditions. *J. Nucl. Mater.* v. 210 p. 244-253.
- Trinkaus, H., Singh, B.N., Woo, C.H. (1994). Defect accumulation under cascade damage conditions. *J. Nucl. Mater.* v. 212/215 p. 18-28.
- Zinkle, S.J., Horsewell, A., Singh, B.N., Sommer, W.F. (1994). Defect microstructure in copper alloys irradiated with 750 MeV protons. *J. Nucl. Mater.* v. 212/215 p. 132-138. Singh, B.N. (1994). Assessment of physical, mechanical and technological properties of first candidate copper alloys. *Risø-R-769 (EN)*, September 1994, 55 pages.

3.4.2 Conference Contributions

- Singh, B.N. (1994). Assessment of Radiation Damage Effects in an Environment of Fusion Neutrons, International Workshop on "20 Years of Progress in Fusion Materials", JRC, Ispra, Italy (March).
- Eldrup, M. (1994). Positron Methods for the Study of Defects in Bulk Materials, Industrial Applications of Positron Annihilation. Europhysics Industrial Workshop, Oisterwijk, The Netherlands (March).
- Eldrup, M. (1994). Defects and Fundamentals. Summary Talk. Proc. 10th International Conference on Positron Annihilation, Beijing, China (May).

- Singh, B.N., Evans, J.H., Horsewell, A., Toft, P. and Edwards, D.J. (1994) "Microstructure and Tensile Properties of TZM and Mo-5% Re Alloys Irradiated with Fission Neutrons, ASTM, 17th Symposium on Effects of Radiation on Materials, Sun Valley, U.S.A. (June).
- Singh, B.N., Horsewell, A.H., Toft, P. and Edwards, D.J. (1994) Temperature and Dose Dependencies of Tensile Properties and Microstructure of Neutron Irradiated OFHC-Copper, ASTM, 17th Symposium on Effects of Radiation on Materials, Sun Valley (June).
- Singh, B.N., Eldrup, M., Horsewell, A., Ehrhart, P. and Dworschak, F. (1994). Differences in Void Swelling Behaviour of Copper Irradiated with 2.5 MeV Electrons and Fission Neutrons, ASTM, 17th Symposium on Effects of Radiation on Materials, Sun Valley, U.S.A. (June).
- Heinisch, H.L. and Singh, B.N. (1994). Differential Defect Production in High Energy Cascades, ASTM, 17th Symposium on Effects of Radiation on Materials, Sun Valley, (June).
- Singh, B.N. (1994). Damage Production and Accumulation during Irradiation: An Overview, International Workshops on An Assessment of Fundamental Aspects of Radiation Damage Production and Accumulation in Metals and Alloys, Obninsk, Russia (September).
- Woo, C.H. and Singh, B.N. (1994). Modelling Irradiation Damage Effects under Cascade Damage Conditions, International Workshop on Assessment of Fundamental Aspects of Radiation Damage Production in Accumulation in Metals and Alloys, Obninsk, Russia (September).
- Golubov, S.I., Singh, B.N., Barrashev, A.V. and Bankrashkov, A.V. (1994). Cascade-Induced Production Bias, International Workshop on An Assessment of Fundamental Aspects of Radiation Damage Production and Accumulation in Metals and Alloys, Obninsk, Russia (September).
- Dai, J., Paschoud, F., Victoria, M. and Singh, B.N. (1994). The Effect of Recoil Energy Spectrum on the Microstructure and Mechanical Properties of Metals, International Workshop on An Assessment of Fundamental Aspects of Radiation Damage Production and Accumulation in Metals and Alloys, Obninsk, Russia (September).
- Zinkle, S.J., Singh, B.N. and Edwards, D.J.(1994). Effect of Intracascade clustering on Defect Accumulation and Pattern Formation in Neutron Irradiated Copper and Nickel. International Workshop on An Assessment of Fundamental Aspects of Damage Production and Accumulation in Metals and Alloys, Obninsk, Russia (September).
- Singh, B.N. (1994). Pre- and Post-Irradiation Properties of Copper and Copper Alloys, ITER-Technical Meeting on Irradiation Testing of In-Vessel Structural Materials and Components, Garching Joint Work Site, Germany (December).
- Singh, B.N. and Woo, C.H. (1994). Consequences of Intracascade clustering on defect accumulation and materials Performance. Ishino Conference on Fundamentals of Radiation Damage and Challenges for Future Nuclear Materials, University of Tokyo, Tokyo, Japan (December).

Title and author(s)

Association Euratom - Risø National Laboratory
Annual Progress Report 1994

J.P. Lynov, P. Michelsen, and B.N. Singh

ISBN	ISSN
87-550-2084-4	0106-2840

Dept. or group	Date
Optics and Fluid Dynamics Department	June 1995

Groups own reg. number(s)	Project/contract No.
---------------------------	----------------------

Pages	Tables	Illustrations	References
50		20	19

Abstract (Max. 2000 char.)

The program of the Research Unit of the Fusion Association Euratom - Risø National Laboratory covers work in fusion plasma physics and in fusion technology. The fusion plasma physics group has activities within (a) studies of nonlinear dynamical processes in magnetized plasmas, (b) development of laser diagnostics for fusion plasmas, and (c) development of pellet injectors for fusion experiments. The activities in technology cover (a) radiation damage of fusion reactor materials and (b) water radiolysis under ITER conditions. A summary of the activities in 1994 is presented.

Descriptors INIS/EDB

LASER DOPPLER ANEMOMETERS; MAGNETIC CONFINEMENT; NON-LINEAR PROBLEMS; NUMERICAL SOLUTION; PELLET INJECTION; PLASMA DIAGNOSTICS; PLASMA SCRAPE-OFF LAYER; PLASMA SIMULATION; PROGRESS REPORT; RISØ NATIONAL LABORATORY; THERMONUCLEAR REACTOR MATERIALS; TOKAMAK DEVICES; TURBULENCE; VORTICES

Available on request from:

Information Service Department, Risø National Laboratory (Afdelingen for Informationservice, Forskningscenter Risø)

P.O. Box 49, DK-4000 Roskilde, Denmark

Phone (+45) 46 77 46 77, ext. 4004/4005 · Telex 43 116 · Telefax (+45) 46 75 56 27



Objective

The objective of Risø's research is to provide industry and society with new potential in three main areas:

- *Energy technology and energy planning*
- *Environmental aspects of energy, industrial and plant production*
- *Materials and measuring techniques for industry*

As a special obligation Risø maintains and extends the knowledge required to advise the authorities on nuclear matters.

Research Profile

Risø's research is long-term and knowledge-oriented and directed toward areas where there are recognised needs for new solutions in Danish society. The programme areas are:

- *Combustion and gasification*
- *Wind energy*
- *Energy technologies for the future*
- *Energy planning*
- *Environmental aspects of energy and industrial production*
- *Environmental aspects of plant production*
- *Nuclear safety and radiation protection*
- *Materials with new physical and chemical properties*
- *Structural materials*
- *Optical measurement techniques and information processing*

Transfer of Knowledge

The results of Risø's research are transferred to industry and authorities through:

- *Research co-operation*
- *Co-operation in R&D consortia*
- *R&D clubs and exchange of researchers*
- *Centre for Advanced Technology*
- *Patenting and licencing activities*

To the scientific world through:

- *Publication activities*
- *Co-operation in: national and international networks*
- *PhD- and Post Doc. education*

Risø-R-830(EN)
ISBN 87-550-2084-4
ISSN 0106-2840

Available on request from:
Information Service Department
Risø National Laboratory
P.O. Box 49, DK-4000 Roskilde, Denmark
Phone +45 46 77 46 77, ext. 4004/4005
Telex 43116, Fax +45 46 75 56 27

Key Figures

Risø has a staff of just over 900, of which more than 300 are scientists and 80 are PhD and Post Doc. students. Risø's 1995 budget totals DKK 476m, of which 45% come from research programmes and commercial contracts, while the remainder is covered by government appropriations.